Order Number 9210961

Asymptotic description of the acoustic microscopy of a surface-breaking crack

Rebinsky, Douglas Alexander, Ph.D.

University of Illinois at Urbana-Champaign, 1991

U·M·I
300 N. Zeeb Rd.
Ann Arbor, MI 48106

ASYMPTOTIC DESCRIPTION OF THE ACOUSTIC MICROSCOPY OF A SURFACE-BREAKING CRACK

BY

DOUGLAS ALEXANDER REBINSKY

B.Sc., University of Alberta, 1984
M.Sc., University of Alberta, 1986

THESIS

Submitted in partial fulfillment of the requirements
for the degree of Doctor of Philosophy in Theoretical and Applied Mechanics
in the Graduate College of the
University of Illinois at Urbana-Champaign, 1991

Urbana, Illinois

UNIVERSITY OF ILLINOIS AT URBANA-CHAMPAIGN

THE GRADUATE COLLEGE

JULY 1991

WE HEREBY RECOMMEND THAT THE THESIS BY

DOUGLAS ALEXANDER REBINSKY

ENTITLED ASYMPTOTIC DESCRIPTION OF THE ACOUSTIC MICROSCOPY OF A SURFACE-BREAKING CRACK

BE ACCEPTED IN PARTIAL FULFILLMENT OF THE REQUIREMENTS FOR THE DEGREE OF DOCTOR OF PHILOSOPHY

John G. Harris
Director of Thesis Research

Arnold E. Carlson
Head of Department

Committee on Final Examination†

John G. Harris
Chairperson

Christopher J. Lawrence

William D. O'Brien Jr.

Steven J. Franke

† Required for doctor's degree but not for master's.

O-517

ABSTRACT

An asymptotic description of the acoustic signature of a crack, breaking the surface of an otherwise homogeneous, isotropic elastic material, determined using either a line focus or a point focus scanning acoustic microscope is constructed. The incident focused beam is constructed as a Fourier integral that produces a specified profile in the focal plane. The wavefields scattered from the specimen are also represented as Fourier integrals. Because the lenses of the acoustic microscopes are characterized by a large Fresnel number and a F-number of order one, the Fourier integrals can be asymptotically approximated to obtain explicit expressions for the incident wavefield and the wavefield scattered from a defect-free surface. The latter wavefield contains the leaky Rayleigh wave that is incident to the surface-breaking crack. The surface-breaking crack is characterized by assigning it reflection and transmission coefficients. The wavefield scattered from the crack is estimated by tracing the leaky Rayleigh waves reflected and transmitted by the crack. Lastly, the acoustic signature is calculated by using the approximate incident and scattered wavefields in an electromechanical reciprocity identity that links the voltage measured at the microscope's transducer to the scattered acoustic wavefields at the surface of the specimen. Expressions for the acoustic signatures made using the line focus and point focus microscopes are compared. Moreover, from the expression for the acoustic signature, the leaky Rayleigh wave reflection and transmission coefficients can be extracted.

But, my Nina, on the morrow,

By the fire's unsteady blaze,

I will drown my gloom, my sorrow

And my dullness in your gaze.

from *Wintry Road*

Alexander S. Pushkin, 1826

ACKNOWLEDGMENTS

I would like to acknowledge gratefully the many individuals who contributed to the success of this research. I am most indebted to Prof. John G. Harris for his continuing patience, guidance and thoughtful insight throughout this study. I greatly appreciate the many informative discussions covering the intricacies of acoustics with Prof. W.D. O'Brien and Nadine B. Smith of the Bioacoustics Lab at the University of Illinois. I am grateful for the financial support from my parents, the Manufacturing Research Center at the University of Illinois and the teaching assistantships provided by the Department of Theoretical and Applied Mechanics. Also, I would like to thank Dr. J.O. Kim at CQEFP at Northwestern University for providing the experimental acoustic signature for fused quartz.

Additionally, I must credit my family and close friends whose unyielding encouragement carried me through the difficult times of the past few years. Lastly, without their support, this effort could not have been finished. And most of all, I thank Nina A. Sluz for so many special things that had nothing - and yet everything - to do with the completion of this thesis.

Table of Contents

CHAPTER 1

Scanning Acoustic Microscopy

1.1 Introduction

The micromechanical properties of surfaces and near surface regions play a pivotal role in determining the strength and other mechanical properties of parts having a high surface to bulk ratio. For example, the micromechanical properities of ceramic surfaces such as hardness, indentation fracture toughness and resistance to wear are largely influenced by the behavior of small flaws breaking at or lurking beneath the surface. The scanning acoustic microscope has an ability to detect such flaws even though their lengths may be only tens of micrometers (Lawrence, *et al.*, 1990)[1].

Both a point focus and a line focus scanning acoustic microscope are available. These devices use a focused beam to scan a surface both horizontally and vertically. The focused beam excites leaky Rayleigh waves as well as a geometrically reflected wave so that the scans exhibit interference patterns from which quantitative information can be inferred. The voltage output of the microscope's transducer as a function of position, as the microscope scans horizontally and vertically, is called the acoustic signature of the surface and its features. The purpose of this research is to explore how the microscope can be used to acquire quantitative information about surface-breaking cracks from the acoustic signature by asymptotically calculating the wave interactions taking place.

[1] References are listed alphabetically at the end of the thesis.

Lemons and Quate (1979) give useful reviews of acoustic microscopy and its applications. An overview on the operation and techniques of acoustic microscopy is provided by Briggs (1985). Specific information about the line focus microscope and its measurement capabilities is given by Kushibiki and Chubachi (1985). Visualization of the ultrasonic pulses in both the coupling fluid and the solid using an optical glass model of a line focus scanning acoustic microscope are shown in Li and Negishi (1989).

Several approaches to modeling the acoustic signature have been used. Bertoni (1984) uses a ray theory to model the acoustic signature of a defect-free surface. In this approach, rays are traced through the microscope to its transducer. Liang, *et al.* (1985a) use an electromechanical reciprocity relation, described by Auld (1979), to relate the acoustic wavefields in the coupling fluid to the voltage output of the microscope's transducer. In this way they calculate the acoustic signature for a point focus microscope of a defect-free surface from only a knowledge of the wavefields at the surface. Achenbach, *et al.* (1991) employ this same general approach to calculate the acoustic signature for a line focus microscope of a defect-free surface using the boundary element method. They calculate not only the acoustic wavefields scattered from the surface, but also the effects of the lens and its coating upon the incident wavefield. Ahn, *et al.* (1991) extend the work of Achenbach, *et al.* (1991) to calculate the acoustic signature for a surface-breaking crack. To take account of a surface-breaking crack, Somekh, *et al.* (1985) and Li, *et al.* (1991) describe a model for the acoustic signature for the line focus microscope that entails calculating a scattering function in the spatial Fourier transform domain. Then they propagate the spectrum of the combined geometric and leaky wave contributions back to the transducer using a transfer function characterizing the microscope.

Because a leaky Rayleigh wave contributes significantly to the acoustic signature, the scanning acoustic microscope is particularly sensitive to vertical discontinuities such as

surface-breaking cracks. Indications of such discontinuities differ somewhat depending upon whether the microscope is near or far from the discontinuity. Yamanaka and Enomoto (1982), using a point focus microscope, observed ripples running parallel to a crack and having a periodicity of approximately one half a Rayleigh wavelength when the microscope was not directly over the crack. They were observing a standing wave pattern formed from the interference of the incident and the reflected leaky Rayleigh waves. Ilett, *et al.* (1984), also using a point focus microscope, observed that vertical discontinuities whose openings were considerably smaller than an acoustic wavelength (in water) were strongly imaged when the microscope was over the discontinuity.

When a Rayleigh wave, guided by either a free or fluid-loaded surface, strikes a surface-breaking crack, a complicated set of waves is scattered from it. However, away from the crack opening, it is possible to define reflection and transmission coefficients for the Rayleigh waves. Achenbach, *et al.* (1980) undertook a geometrical elastodynamic analysis of how a Rayleigh wave which is normally incident to a crack breaking a free surface will scatter. However, to date most studies of this problem have been done numerically or experimentally, and moreover, they have been done for surfaces free of fluid loading. Angel and Achenbach (1984) computed reflection and transmission coefficients for a Rayleigh wave obliquely incident to a surface-breaking crack, and Dong and Adler (1984) measured these coefficients, getting good agreement with the calculations of Angel and Achenbach (1984). Using these same reflection and transmission coefficients, Rowe *et al.* (1986) were able to get limited agreement between the theoretical work of Somekh, *et al.* (1985) and the measurements of the output of a scanning acoustic microscope.

1.2 An Asymptotic Model of the Microscope

Figure 1.1 shows the geometry of the acoustic microscope. The microscope consists of a buffer rod with a transducer at one end and a lens at the other. The ultrasound radiated from the lens is coupled to the surface of a solid half-space by a fluid, usually water. The transducer radiates a tone burst, so that the delay introduced by the buffer rod allows the signals to be separated provided the pulse length is sufficiently short. Therefore, the wavefields are taken to be time-harmonic, suppressing the $\exp(-i\omega t)$ in the calculation. Also, the scattered wavefield is considered to be that scattered from the interface once, assuming that any multiply scattered wavefields are separated in time.

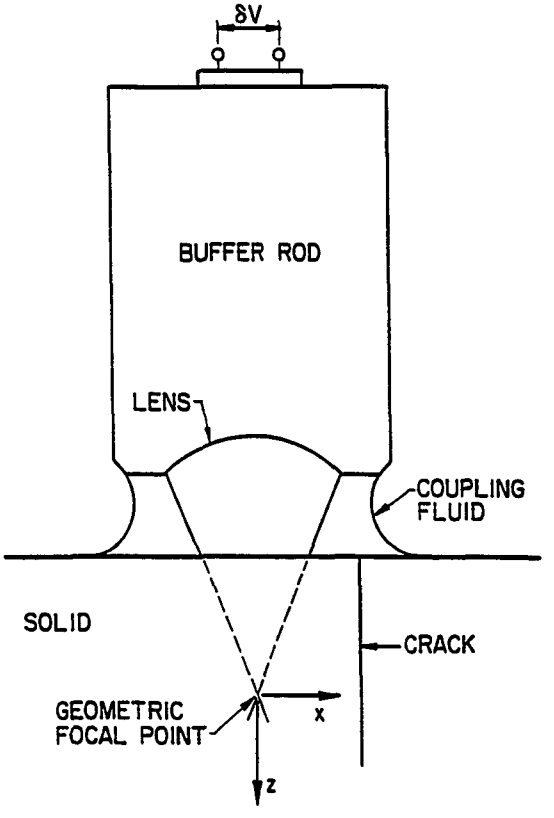

Fig. 1.1 A diagram of the overall features of a scanning acoustic microscope and the specimen.

To relate the voltage change δV caused by the presence of a solid surface to the acoustic wavefields in the fluid couplant, an electromechanical reciprocity identity (Auld, 1979) is used. It is assumed that the solid is homogeneous, isotropic and linearly elastic, and that the fluid is ideal with the exception of section 2.4. Application of this reciprocity identity gives

$$\delta V = \tilde{C} \int_S \left(\frac{\partial \phi^i}{\partial n} \phi^s - \phi^i \frac{\partial \phi^s}{\partial n} \right) dS \tag{1.1}$$

where ϕ is the displacement potential in the fluid and the superscripts i and s indicate the incident and the scattered wavefields. The voltage change δV has been normalized with a constant which is proportional to the time-averaged incident complex power, as adopted by Liang, *et al.* (1985a).

$$\frac{1}{\tilde{C}} = 2 \int_S \frac{\partial \phi^i}{\partial n} \phi^{i^*} dS \tag{1.2}$$

The * indicates that the complex conjugate is to be taken. The surface is one that lies between the plane of the lens' aperture and the solid surface and the normal points in the positive z direction (Fig. 1.1). Note that the pressure $p = \rho_f \omega^2 \phi$, where ρ_f is the fluid density and ω is the angular frequency, and the particle displacement $\vec{u} = \vec{\nabla} \phi$.

This research is largely concerned with how to calculate the quantities in the integrand of Eq. (1.1).

CHAPTER 2

Line Focus Microscope

2.1 The Incident Wavefield

To construct the incident focused wavefield, the Debye approximation (Stamnes, 1986, pp. 243-281 and 377-389) is used. Figure 2.1 shows the geometry for the incident wavefield. The incident wavefield ϕ^i is given by

$$\phi^i = \frac{1}{ik^2\sqrt{2\pi}} \int_{-\beta_a}^{\beta_a} E(\beta) \exp[\pm i 2\pi F N(\bar{x}\sin\beta + F|\bar{z}|\cos\beta)] d\beta \tag{2.1}$$

where the minus sign indicates a disturbance incoming to the focal plane, and the plus sign represents one which is outgoing. The coordinate $\bar{x} = x/b$ and $\bar{z} = z/f$, where f is the focal length defined in Fig. 2.1. The terms F and N are the F-number and the Fresel number respectively and they are defined below. k is the wave number in the fluid. The amplitude function $E(\beta)$ and the possibly complex angle β_a remain to be determined. Note that in the focal plane $\phi^i(x,0)$ is the Fourier transform of $E(\beta)$.

There are two parameters that characterize a focused beam (Stamnes, 1989, pp. 398-409). These are the Fresnel number N and the F-number F where

$$N = \frac{kb^2}{2\pi f} \tag{2.2}$$

and

$$F = f/b\,. \tag{2.3}$$

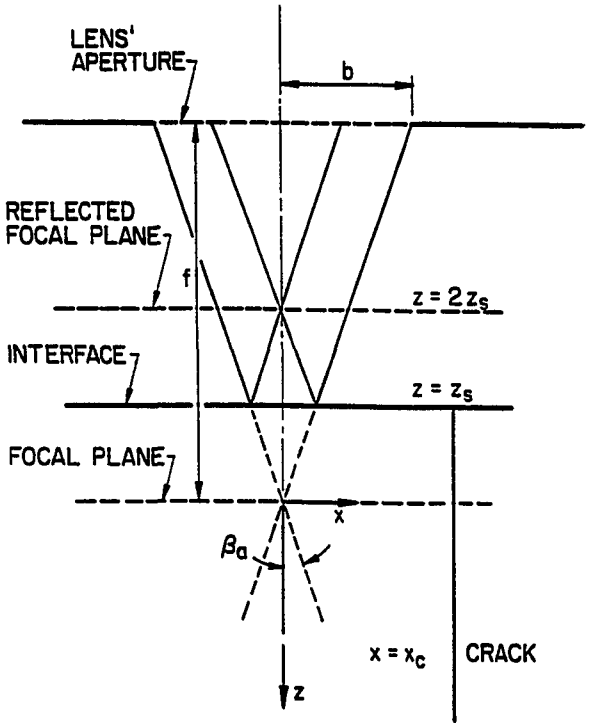

Fig. 2.1. The geometrical features of the incident and scattered acoustic beams. Note that the geometrical focal point is the origin of the coordinate system.

In this work, the F-number is chosen to be written in terms of the radius of the aperture. This is different than the convention of using the diameter. Note that the parameter kb can be written as $kb = 2\pi FN$. The cases in which $F = O(1)$ and N is large are of interest. Thus kb is large. Accordingly, the integral in Eq. (2.1) is readily approximated asymptotically, giving

$$\phi^i = -\frac{E(\Theta)}{k^2}\frac{\left[\pm\exp\left(\pm ikR \pm i\frac{\pi}{4}\right)\right]}{\sqrt{kR}} \tag{2.4}$$

where $R = \sqrt{x^2+z^2}$, $x = |z|\tan\Theta$ and $|\Theta| \le \pi/2$.

To determine $E(\beta)$ and β_a, it is demanded that ϕ^i asymptotically matches a given ϕ^i at the lens' aperture $z = -f$. Note that the aperture of the lens of an acoustic microscope does not end abruptly so that edge-diffracted waves are not expected to be strongly excited. Accordingly, the following aperture distribution is proposed for $|x| \le b$:

$$\phi^i = \frac{A}{k^2} \exp\left[-\left(\frac{b}{a} \frac{x}{b} \right)^{2n} \right] \frac{\exp(-ikR_0)}{\sqrt{kR_0}} \tag{2.5}$$

where A is an amplitude constant, a is a parameter that measures how fully the beam fills the aperture and n is an integer greater than or equal to unity that determines how abruptly the distribution falls off at a. The distance $R_0 = \sqrt{x^2 + f^2}$. If b is allowed to go to infinity, the distribution goes to zero at the edges. If b is finite, provided $a/b < 1$, the magnitude of the distribution is small at b.

Equating the asymptotic approximations to ϕ^i, Eqs. (2.4) and (2.5), gives

$$E(\beta) = A \exp\left[-\left(F \frac{b}{a} \tan\beta \right)^{2n} \right] \exp\left(i \frac{\pi}{4} \right). \tag{2.6}$$

The angle $\beta_a = \tan^{-1} F$. Figure 2.2 shows transverse profiles for the acoustic beam, radiated into the fluid at the plane of the lens' aperture, for n = 1, 2 and 4, and a/b = 0.50, 0.75 and 0.85, respectively. The frequency of operation is 225 MHz. The fluid is water which has a density of 998 kg/m^3 and a wavespeed of 1480 m/s. The Fresnel number equals 178 and the F-number equals 0.753.

Note that in all cases the wavefield is not large at the edges. In section 2.3, the asymptotic expression for $|\delta V|$ is compared with a measured result for fused quartz using a microscope

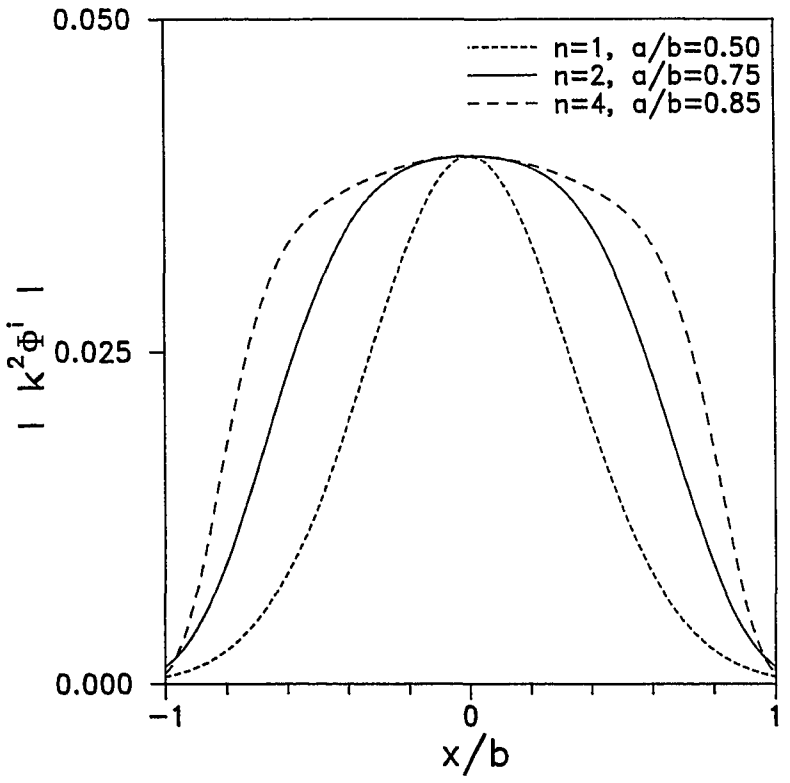

Fig. 2.2 Transverse profiles along the lens' aperture of the acoustic beam radiated into the fluid.

operating at the same frequency and having the same Fresnel number and F-number. There it is found that the profile with $n = 2$ and $a/b = 0.75$ gives the best overall fit. Thus, this profile will be used for numerical examples concerning the line focus microscope.

2.2 The Scattered Wavefield for a Defect-Free Surface

Figure 2.1 also shows the geometry for the scattered wavefield. Note that $z = z_s$ gives the position of the interface between the solid and the coupling fluid relative to the geometrical focal point. Because the incident wavefield is expressed as an angular spectrum, the scattered wavefield ϕ^s is readily constructed giving

$$\phi^s = \frac{1}{ik^2\sqrt{2\pi}} \int_{-\beta_a}^{\beta_a} E(\beta) R(\beta) \exp[\pm i 2\pi FN(\bar{x}\sin\beta + F|\bar{z} - 2\bar{z}_s|\cos\beta)]\, d\beta \tag{2.7}$$

where the minus sign indicates a disturbance incoming to the reflected focal plane, at $z = 2z_S$, and the plus sign one which is outgoing. The term $R(\beta)$ is the plane-wave reflection coefficient for the displacement potential for a fluid-solid interface and is given in Brekhovskikh (1980, pp. 41-50). It has four poles and four branch points in the complex β-plane, each of which gives rise to a surface disturbance (Pott and Harris, 1984). While other leaky surface waves may contribute to the acoustic signature, it is the leaky Rayleigh waves that are most strongly excited, provided β_a is sufficiently large (Harris and Pott, 1985). The structure of $R(\beta)$ and of the complex β-plane is discussed further in Appendix A.

The basic physical components of Eq. (2.7) are exhibited by a non-uniform asymptotic approximation, namely

$$\begin{aligned} k^2\phi^s = & -E(\theta)R(\theta)\frac{\exp(\pm ikr)}{\sqrt{kr}}\left[\pm\exp\left(\pm i\frac{\pi}{4}\right)\right] \\ & + u[\pm(\theta-\beta_r)]\, 2i\alpha_r\sqrt{2\pi}E(\beta_r)\exp[\pm ikr\cos(\theta-\beta_p)] \\ & + u[\pm(-\theta-\beta_r)]\, 2i\alpha_r\sqrt{2\pi}E(\beta_r)\exp[\pm ikr\cos(\theta+\beta_p)] \end{aligned} \tag{2.8}$$

and the coordinates r and θ are given by

$$x = r\sin\theta \tag{2.9}$$

and

$$|z - 2z_s| = r\cos\theta \tag{2.10}$$

where $|\theta| \leq \pi/2$. The Rayleigh pole is given by $\beta_p = \beta_r + i\alpha_r$. The α_r indicates that the wave is leaky, and does not indicate an attenuation caused by viscosity or any other loss mechanism in the fluid or solid. Not only does it have poles at $\pm\beta_p$, but $R(\beta)$ also has zeros at $\pm\beta_p^*$ (Bertoni, 1984), where * indicates the complex conjugate. Using this fact, the residue of the reflection coefficient can be approximated as (Somekh, *et al.*, 1985)

$$A_-(\pm\beta_p)/\frac{dA_+}{d\beta}(\pm\beta_p) \quad \cong \quad \pm 2i\alpha_r \tag{2.11}$$

where A_- is the numerator and A_+ is the denominator of $R(\beta)$ [Eqs. (A1) - (A3)]. Because α_r is small, β_p has been approximated by β_r in the amplitude terms. The function $u(x)$ is the Heaviside function. The first term in Eq. (2.8) is the geometrical one, while the second and third represent the leaky Rayleigh waves. Note that to excite the Rayleigh wave strongly β_a must be greater than β_r.

Figure 2.3 shows the transverse profile for the scattered wavefield calculated using Eq. (2.8) at the plane of the lens' aperture $z = -f$, where the geometrical component has undergone sufficient geometrical decay that the presence of the Rayleigh wave is clear. The solid is fused quartz, whose density, longitudinal wavespeed and transverse wavespeed are 2200 kg/m^3, 5960 m/s and 3760 m/s, respectively. The remaining parameters are those used in the previous figure, and as mentioned earlier, the incident beam profile is described by $n = 2$ and $a/b = 0.75$. The strong oscillations at each side indicate the strong influence of the leaky Rayleigh wave on the signal collected by the lens. Interestingly, the two smaller spikes nearest the axis $x/b = 0$ are caused by reflection at the angle of critical refraction for the longitudinal wave. Recently, Chan and Bertoni (1991) studied the effect of the longitudinal lateral wave upon the scattered wavefield and the acoustic signature.

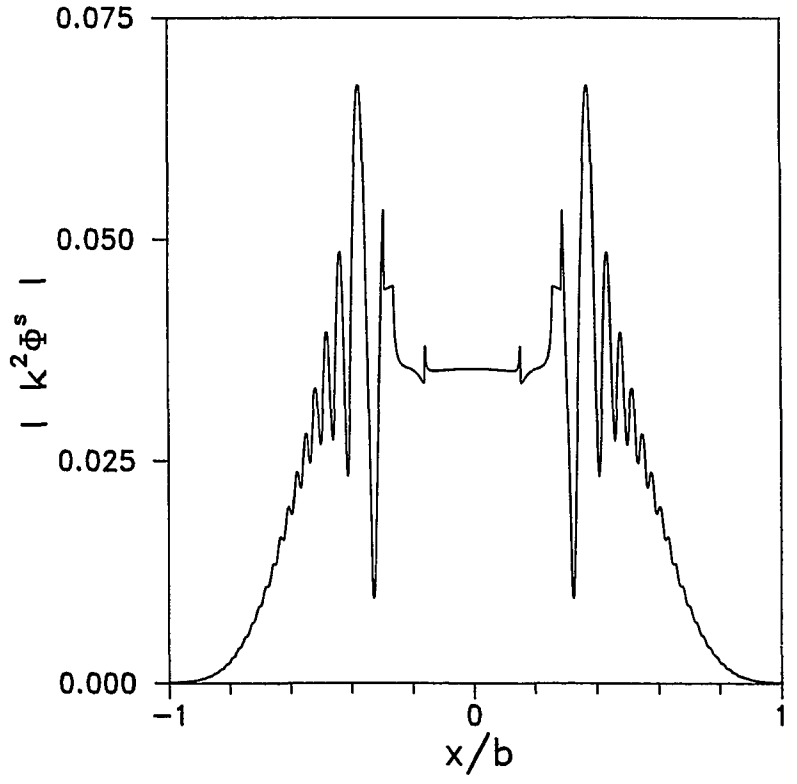

Fig. 2.3 Transverse profile along the lens' aperture of the scattered wavefield for fused quartz at a defocus of $z_s/\lambda_w = -10$. Incident profile parameters are $n = 2$ and $a/b = 0.75$.

2.3 The Acoustic Signature for a Defect-Free Surface

Note that both the incident and the scattered wavefields are expressed as Fourier transforms. If these Fourier transforms are substituted directly into the Parseval's relation equilvalent of Eq. (1.1), the expression for the change in voltage can be written as

$$\delta V_o^L = -2iC^L \int_0^{\beta_a} E^2(\beta) R(\beta) \exp(\pm 2ikbF\,|\,\bar{z}_s\,|\cos\beta)\, d\beta \qquad (2.12)$$

with

$$\frac{1}{C^L} = 2i \int_0^{\beta_a} E(\beta) E^*(\beta) d\beta \tag{2.13}$$

where C^L is proportional to $\tilde{C}$ given in Eq. (1.2). The superscript L denotes a line focus microscope. The plus sign is used when the focal point is above the interface and the minus sign is chosen when it is below. The subscript o indicates that the surface is defect-free. This is essentially the same expression as that derived by Liang, *et al.* (1985a). In addition to being quite simple, it contains no reference to the contour of integration S. Further, the integral is readily approximated asymptotically, giving

$$\delta V_o^L = -C^L E^2(0) R(0) \sqrt{\frac{\pi}{k \mid z_s \mid}} \exp(\pm 2ik \mid z_s \mid) \left[\pm \exp\left(\pm i \frac{\pi}{4} \right) \right]$$
$$+ u(-z_s) C^L E^2(\beta_r) 8\pi i \alpha_r \exp(-2ik \mid z_s \mid \cos\beta_p) . \tag{2.14}$$

This expression exhibits the basic physical mechanisms that contribute to the acoustic signature and agrees with the expressions given by Ilett, *et al.* (1984) and Somekh, *et al.* (1985). Note that when the focal point is below the interface the signals caused by the geometric and the leaky Rayleigh wave interfere, giving an interference pattern as z_s is changed. The distance between the maxima $\Delta \mid z_s \mid$ is

$$\Delta \mid z_s \mid = \frac{\pi}{k(1 - \cos\beta_r)} \tag{2.15}$$

where β_p has been approximated by β_r. It is relatively easy to calculate the asymptotic contribution from the endpoint, provided β_a is not close to β_r. That term is $O(1/kb)$, and its strength which is proportional to $E(\beta_a)$, has been ignored.

The acoustic signature can also be calculated by using the asymptotic expressions for ϕ^i and ϕ^s and evaluating Eq. (1.1) along a suitable surface S. Taking S to be the interface is satisfactory except for values of z_s quite close to zero where the focal point lies on the interface. Even in this case it is not a serious problem. The calculation is straightforward though lengthy. The detailed expressions are

$$\delta V_o^L = -(\pm 2C^L)\int_0^{\beta_a} E^2(\beta)R(\beta)\exp(\pm i2kbF\,|\,\bar{z}_s\,|\sec\beta)\,d\beta$$

$$+2C^L\,\alpha_r\,E(\beta_r)\sqrt{2\pi k\,|\,z_s\,|}\left[\pm\exp\left(\pm i\frac{\pi}{4}\right)\right]$$

$$\times\int_{\beta_r,-\beta_a}^{\beta_a,\beta_r} E(\beta_r)\sqrt{\sec\beta}\left(1+\frac{\cos\beta_r}{\cos\beta}\right)$$

$$\times\exp\{\pm ikbF\,|\,\bar{z}_s\,|\sec\beta(\cos(\beta_p-\beta)+1)\}\,d\beta \qquad (2.16)$$

where the plus sign and the first set of integration limits are taken when the focal point is above the interface, and the minus sign and the second set of integration limits are taken when it is below the interface. One can repeat this calculation using the plane of the lens' aperture as the surface S. Interestingly, both yield Eq. (2.14) when they are evaluated asymptotically. For positive defocus $\bar{z}_s > 0$, the pole term in the geometric contribution has been ignored in Eq. (2.16). This term will be small because of the secant in the exponential in the geometric term, for $kbF\,|\,\bar{z}_s\,|$ of moderate size and for an α_r which is not very small. For α_r small, the original asymptotic results are not accurate near β_p so that we cannot expect Eq. (2.16) to give accurate results in this region.

Figure 2.4 shows a plot of $|\,\delta V_o^L\,|$ against z_s/λ_w, where λ_w is the wavelength in water (the choice of λ_w is the common scaling, though f would be more appropriate) calculated in several

ways. The solid line is calculated using the asymptotic result Eq. (2.14), the short dashed line using the spectral expression Eq. (2.12), and the longer dashed line using the integration over the interface, Eq. (2.16). The solid is fused quartz. Also, the values of the various parameters are those used previously. The curves do not agree precisely, but their agreement is nevertheless remarkable.

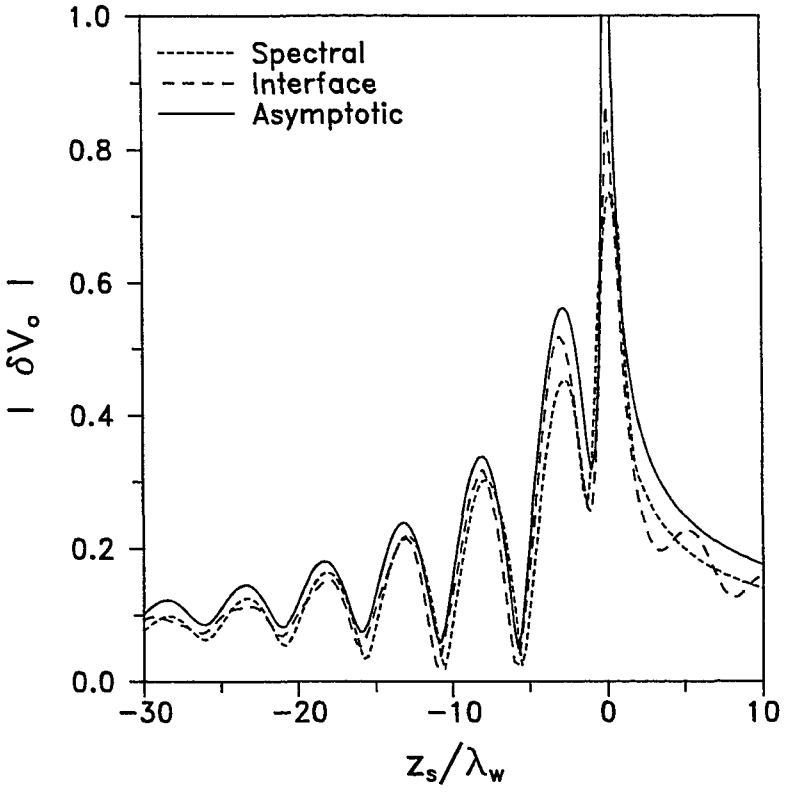

Fig. 2.4 The acoustic signature for fused quartz calculated in three distinct ways.

Figure 2.5 again shows plots of $|\delta V_o^L|$ against z_s/λ_w for fused quartz. The solid curve is an experimental one for a microscope having the same Fresnel number and F-number given earlier,

while the dashed one is calculated from the asymptotic result, Eq. (2.14), using as the incident beam $n = 2$ and $a/b = 0.75$. Again the agreement is quite good, giving us confidence that our asymptotic calculation has captured the essential physical features of the acoustic signature.

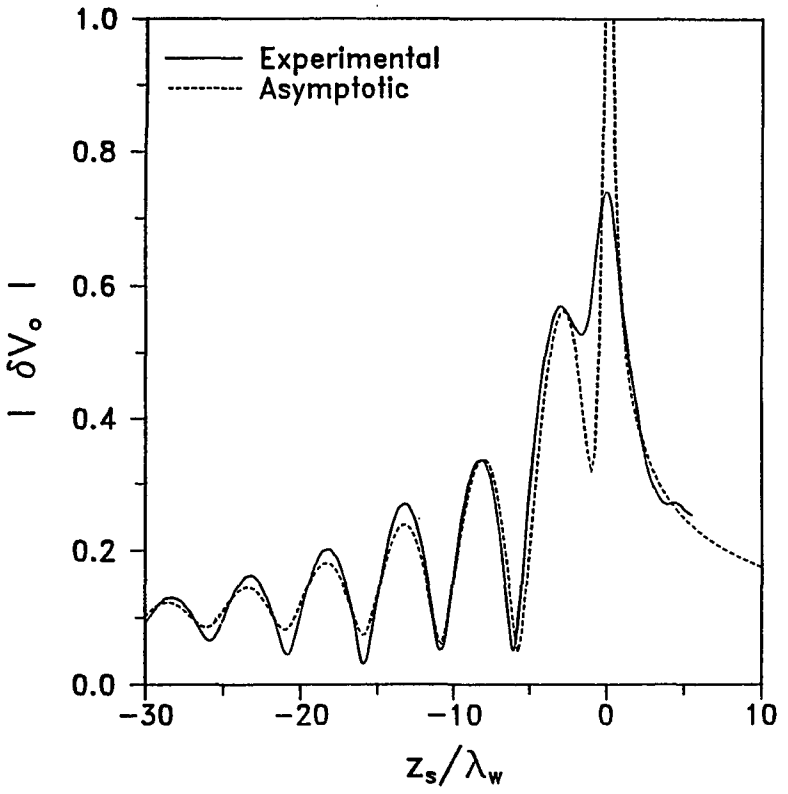

Fig. 2.5 A comparison of the asymptotic expression for the acoustic signature with an experimental acoustic signature for fused quartz.

2.4 Attenuation

At the frequencies of interest here, attenuation is significant. It is assumed that there is attenuation in both the fluid and the solid, and that this attenuation is caused by weak viscosity and possibly heat conduction. Therefore, the attenuation will be proportional to the square of the frequency. It is accounted for by replacing the fluid wavespeed c_f, the longitudinal wavespeed c_L and the transverse wavespeed c_T by c'_f, c'_L and c'_T respectively, where

$$c'_f = c \pm i\omega\alpha_f, \tag{2.17}$$

$$c'_L = c_L \pm i\omega\alpha_L, \tag{2.18}$$

and

$$c'_T = c_L \pm i\omega\alpha_T. \tag{2.19}$$

It is assumed that $|\omega\alpha_n/c_n| \ll 1$ where n indicates f, L or T. The choice of sign requires some care. The incident and the scattered wavefields must decay as they propagate so the plus sign is used for a wavefield propagating toward its focal plane and the minus sign is used as it propagates away.

The behavior of the reflection coefficient $R(\beta)$ when attenuation is included is quite interesting. Without attenuation β_p and β_o, the zero, are the complex conjugates of one another so that in the neighborhood of β_r, $|R(\beta)| = 1$. With attenuation, this symmetry is lost. The pole β_p moves further into the complex plane, while the zero β_o moves toward the real axis so that $|R(\beta)|$ can become quite small in the neighborhood of β_r and its phase behavior complicated (Mott, 1970). However, examining Eq. (2.14) indicates that we need $R(\beta)$ at 0 and β_p. The

coefficient $R(0)$ differs very little from its unattenuated value, and more interestingly at β_p the approximation given by Eq. (2.11) remains accurate. Thus, the attenuation, within the compass of our approximations, affects the exponential terms to greater degree than the amplitudes in Eq. (2.14).

In Fig. 2.6, the asymptotic expressions for $|\,\delta V_o\,|$ with and without attenuation are plotted against z_s/λ_w for a fused quartz half-space. Here $\alpha_f = 1.37\times10^{-9}\,m$, $\alpha_L = 0.117\times10^{-9}\,m$ and $\alpha_T = 0.465\times10^{-9}\,m$. The value for α_T is an estimate. Had only the attenuation in water been considered the attenuated asymptotic result would look no different.

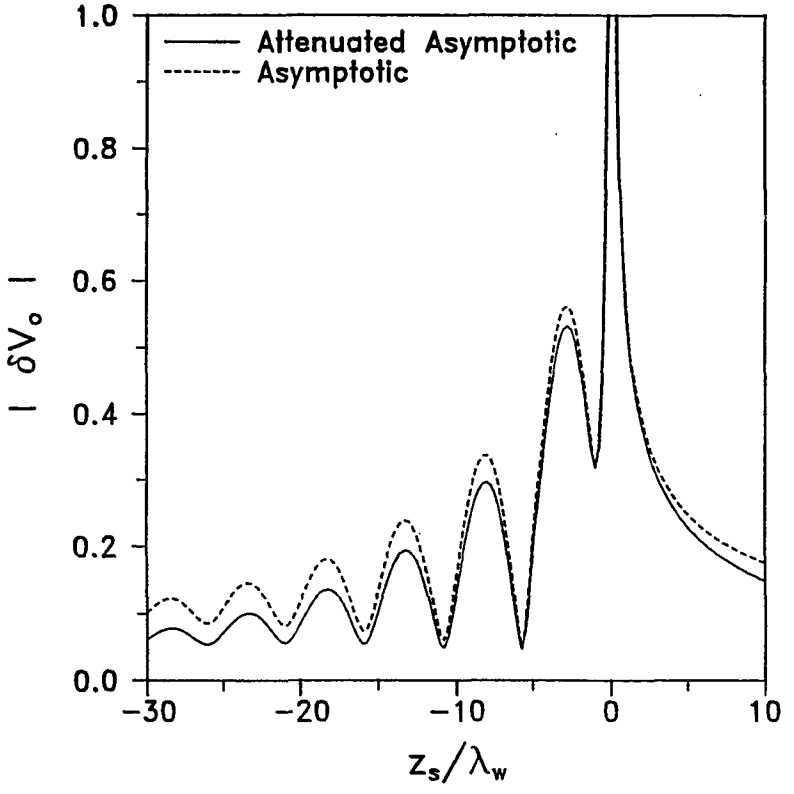

Fig. 2.6 A comparison of the asymptotic expressions, one accounting for attenuation and one not, of the acoustic signature for fused quartz.

There may be other important sources of attenuation such as the acoustic boundary layer at the interface or incoherent scatter from the roughness of the surface. However, unless one wants to measure explicitly attenuation, it is the interference pattern that is of greatest interest, so that attenuation will not be considered further.

2.5 A Surface with a Surface-Breaking Crack

When the focused acoustic beam is scattered from a surface broken by a crack, many scattered disturbances are excited. The specularly reflected signal is strong because reflection causes little diminution in amplitude. The signals diffracted from the crack opening when it is struck directly by the incident beam are unlikely to be strong because the crack openings of interest are less than an acoustic wavelength and asymptotically the diffracted signals are $O(1/\sqrt{kb})$ relative to the reflected one. Accordingly, these signals will be ignored. The leaky Rayleigh waves are expected to interact strongly with the crack because they strike it broadside. As indicated in the introduction of Chap. 1 the interaction is not a simple one. Nevertheless, an examination of the work cited in Chap. 1 suggests that the dominant wave processes are those of reflection and transmission. Thus, it will be assumed that the crack can be characterized by reflection and transmission coefficients and that these are parameters of the model that can be extracted from the acoustic signature.

2.5.1 The Scattered Wavefield

The wavefield scattered from the surface with a surface-breaking crack, considering the approximations just described, consists of Eq. (2.8) plus the terms that take into account the reflection and transmission of the leaky Rayleigh wave by the surface-breaking crack. Let the crack be located at $x = x_c$, where x_c is taken to be positive (Fig. 2.1). Further, let the reflection

and transmission coefficients be the complex parameters R_r and T_r, respectively. For a vertical surface-breaking crack, they are functions of d/λ_r, where d is the crack depth and λ_r is the Rayleigh wavelength, as well as the various material properties. In fact they exhibit an oscillatory behavior with d/λ_r that is a consequence of a standing wave caused by Rayleigh waves travelling down the crack faces, scattering from the crack tip and returning to the surface (Achenbach, *et al.* 1980; Angel and Achenbach, 1984), though there are other wave processes taking place as well. Lastly, let $x_r = |z_s| \tan\beta_r$ indicate the position on the surface where the incident Rayleigh waves are asymptotically excited.

First, considering that the geometrical focal point lies below the interface so that the incident wavefield is incoming, the scattered leaky Rayleigh waves are

$$\begin{aligned} k^2\phi^s_{cr} = {} & 2i\alpha_r E(\beta_r)\sqrt{2\pi}\exp(-ik\,|z-2z_s|\cos\beta_p) \\ & \times[u(x_r-x_c)\{u(x-x_c)R_r\exp[-ik(2x_c-x)\sin\beta_p] \\ & + u(x_c-x)(T_r-1)\exp(-ikx\sin\beta_p)\} \\ & + u(x_c-x)R_r\exp[ik(2x_c-x)\sin\beta_p] \\ & + u(x-x_c)(T_r-1)\exp(ikx\sin\beta_p)]\,. \end{aligned} \tag{2.20}$$

Next, considering that the geometrical focal point lies above the interface so that the incident wavefield is outgoing, the scattered leaky Rayleigh waves are

$$\begin{aligned} k^2\phi^s_{cr} = {} & 2i\alpha_r E(\beta_r)\sqrt{2\pi}\exp(ik\,|z-2z_s|\cos\beta_p) \\ & \times u(x_c-x_r)\{u(x_c-x)R_r\exp[ik(2x_c-x)\sin\beta_p] \\ & + u(x-x_c)(T_r-1)\exp(ikx\sin\beta_p)\}\,. \end{aligned} \tag{2.21}$$

Note that the Heaviside step functions $u(x)$ serve to partition the various regions of the surface in both Eqs. (2.20) and (2.21), and that the (-1) terms are needed to remove the incident Rayleigh waves from regions where they are no longer present. To obtain the net scattered wavefield, one must combine Eq. (2.20) with Eq. (2.8) having the minus sign and for Eq. (2.21) one must add the one having the plus sign.

Figure 2.7 shows a transverse profile for the total scattered wavefield in the plane of the lens' aperture $z = -f$, where the geometrical component has undergone sufficient decay that the presence of the several scattered Rayleigh waves is clear. The solid is fused quartz. The same values for the parameters which have been used in the previous figures are used here. The crack is located at $x_c/b = 0.02$, and the values of R_r and T_r are $0.4\, e^{i0.6}$ and 0, respectively. These values describe a deep crack with no mechanical contact between the faces and they have been taken from Achenbach, *et al.* (1980). Comparison of Fig. 2.7 with Fig. 2.3 shows that the presence of the crack has considerable influence on the scattered wavefield.

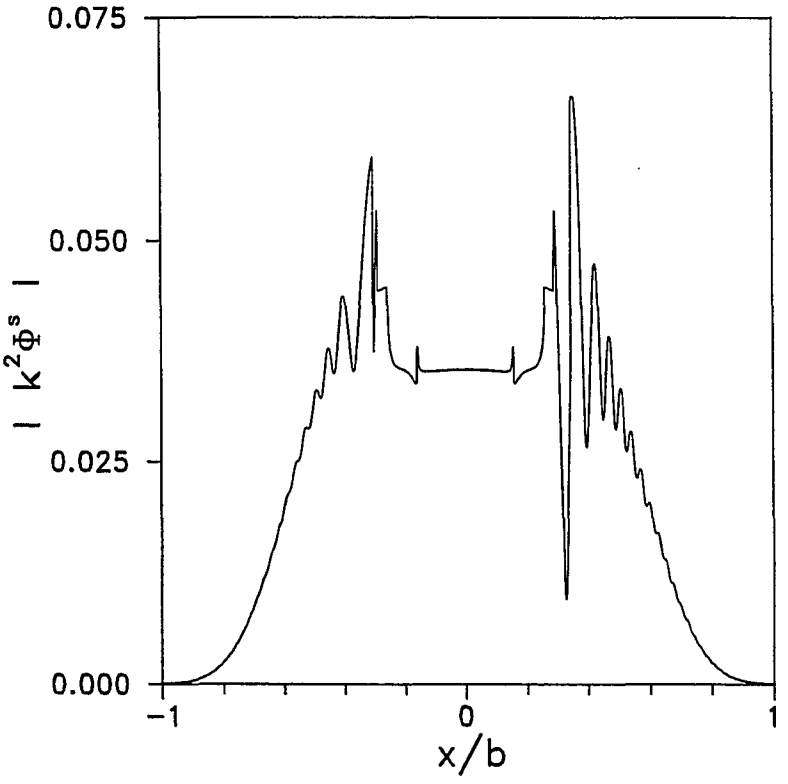

Fig. 2.7 Transverse profile of the scattered wavefield along the lens' aperture at a defocus of $z_s/\lambda_w = -10$ for fused quartz with a surface-breaking crack at $x_c/b = 0.02$. The incident profile parameters are $n = 2$ and $a/b = 0.75$.

2.5.2 The Perturbation to the Acoustic Signature

As Eqs. (2.14) and (2.16) suggest, the acoustic signature can be written as

$$\delta V = \delta V_o + \delta V_{cr} \tag{2.22}$$

where δV_o is the contribution from the geometrically reflected wavefield plus that from the leaky Rayleigh wavefield when no crack is present, and δV_{cr} is the contribution caused by the presence of the crack. Usually, only $|\delta V|$ can be measured because it is difficult to make accurate phase measurements at high frequencies. However, work by Liang, *et al.* (1985b) and Reinholdtsen and Khuri-Yakub (1991) suggests that this problem can be overcome, and that the magnitude and the phase of δV can be measured. If we assume that δV_o is measured in a region of the surface unaffected by Rayleigh waves scattered by the crack, then a measurement of δV allows $|\delta V_{cr}| = |\delta V - \delta V_o|$ to be measured. Using the approximate wavefields, Eqs. (2.20) and (2.21), in combination with an asymptotic approximation to the incident wavefield Eq. (2.1), δV_{cr} is calculated using Eq. (1.1).

The surface S needs to be selected. Both the plane of the lens' aperture and the interface could be used. However, the interface is simpler to work with as done with the defect-free surface acoustic signature calculations. Accordingly, the portion of the total acoustic signature produced by the presence of the surface-breaking crack δV_{cr} is given by the following integral evaluated along the interface for the geometrical focal point located below the surface.

$$\delta V_{cr}^{L} = -C^{L}\alpha_r E(\beta_r)\sqrt{2\pi k\,|\,z_s\,|}\,\exp(-ikbF\,|\,\bar{z}_s\,|\cos\beta_p)\exp\left(-i\frac{\pi}{4}\right)$$

$$\times\int_{-\beta_a}^{\beta_a} E(\beta)\sqrt{\sec\beta}\left(1+\frac{\cos\beta_r}{\cos\beta}\right)\exp(-ikbF\,|\,\bar{z}_s\,|\sec\beta)$$

$$\times[\,u(x_r-x_c)\{u(x-x_c)R_r\exp[-ikb(2\bar{x}_c-\bar{x})\sin\beta_p]$$

$$+u(x_c-x)(T_r-1)\exp(-ikb\bar{x}\sin\beta_p)\}$$

$$+u(x_c-x)R_r\exp[ikb(2\bar{x}_c-\bar{x})\sin\beta_p]$$

$$+u(x-x_c)(T_r-1)\exp(ikb\bar{x}\sin\beta_p)\,]\,d\beta \qquad (2.23)$$

Similiarly, δV_{cr}^{L}, for the geometrical focal point located above the surface, is given by the following integral evaluated along the interface.

$$\delta V_{cr}^{L} = C^{L}\alpha_r E(\beta_r)\sqrt{2\pi k\,|\,z_s\,|}\,\exp(ikbF\,|\,\bar{z}_s\,|\cos\beta_p)\exp\left(i\frac{\pi}{4}\right)$$

$$\times\int_{-\beta_a}^{\beta_a} E(\beta)\sqrt{\sec\beta}\left(1+\frac{\cos\beta_r}{\cos\beta}\right)\exp(ikbF\,|\,\bar{z}_s\,|\sec\beta)$$

$$\times u(x_c-x_r)\{u(x_c-x)R_r\exp[ikb(2\bar{x}_c-\bar{x})\sin\beta_p]$$

$$+u(x-x_c)(T_r-1)\exp(ikb\bar{x}\sin\beta_p)\}\,d\beta \qquad (2.24)$$

In these expressions, $x = |\,z_s\,|\tan\beta$ and x_c, x_r were defined earlier. Note that the singularity in the incident wavefield has disappeared, but the fact that the focal point has crossed the interface is indicated by the $\pi/2$ phase shift. Also, in contrast to similiar expressions given by Somekh, *et al.* (1985) and Li, *et al.* (1991), these are given as integrals in physical space instead of wavenumber space.

The exponential terms in the expressions for δV_{cr}, Eqs. (2.23) and (2.24), have been scaled in order that we may asymptotically approximate them. The earlier work with the defect-free surface suggests that such approximations are accurate. Doing so gives, for the focal point below the interface,

$$\begin{aligned}\delta V_{cr}^{L} = 4\pi i C^{L}\, \alpha_r E^2(\beta_r) \exp(-i2k \mid z_s \mid \cos\beta_p) \\ \times \{R_r [\exp(i2kx_c \sin\beta_p) + u(x_r - x_c)\exp(-i2kx_c \sin\beta_p)] \\ + 2u(x_r - x_c)(T_r - 1)\}\end{aligned} \tag{2.25}$$

while for the focal point above the interface

$$\delta V_{cr}^{L} = 4\pi i C^{L}\, \alpha_r E^2(\beta_r) \exp(i2k \mid z_s \mid \cos\beta_p)\, R_r\, u(x_c - x_r) \exp(i2kx_c \sin\beta_p)\,. \tag{2.26}$$

In Figures 2.8 through 2.11 which concern the crack perturbed acoustic signature, numerical evaluation of Eqs. (2.23) and (2.24) is compared to their asymptotic approximations given in Eqs. (2.25) and (2.26). The material is fused quartz in all cases. Figures 2.8 and 2.10 illustrate that part of the acoustic signature caused the presence of the surface-breaking crack $\mid \delta V_{cr} \mid$ as x_c/b is varied. Figures 2.9 and 2.11 show the dependence of the difference in the magnitudes of the total crack perturbed output voltage and that of a defect-free surface ($\mid \delta V \mid - \mid \delta V_o \mid$) on the position of the surface-breaking crack x_c/b. In Figs. 2.8 and 2.9, the microscope is at a defocus of $z_s/\lambda_w = 5$, while in Figs. 2.10 and 2.11 the defocus is $z_s/\lambda_w = -10$.

The crack reflection and transmission coefficients for a leaky Rayleigh wave used in these figures are $R_r = 0.4\, e^{i0.6}$ and $T_r = 0$ which are identical to those used in Fig. 2.7. Recall that these coefficients approximate those for a deep crack whose faces are not in mechanical contact. Despite their simplicity, the choice of these coefficients gives a good overall picture of how $\mid \delta V_{cr} \mid$ depends on each. The crack reflection coefficient R_r primarily affects the oscillation of

the signal as seen in the first term of Eq. (2.25) while the crack transmission coefficient T_r affects the magnitude of the signal for $x_c < x_r$ as observed in the second term of Eq. (2.25). This is illustrated in Figs. 2.10 and 2.11. For $x_c > x_r$, the signal $|\delta V_{cr}|$ is dependent on only the crack reflection coefficient as noted in Eq. (2.26) and Figs. 2.8 and 2.9. These results reproduce the dependence of the crack perturbed acoustic signature on the crack reflection and transmission coefficients as experimentally observed and explained by Rowe, *et al.* (1986).

The asymptotic approximations, Eqs. (2.25) and (2.26), of the crack perturbed acoustic signature $|\delta V_{cr}^{L}|$ compare favorably with the numerical integration of Eqs. (2.23) and (2.24) as observed in Figs. 2.8 and 2.10. The agreement is quite good for $x_c < x_r$ except in Fig 2.8 where the asymptotic expression has a larger instantaneous jump because of the non-uniform solution. For Fig. 2.10, the oscillation in the decaying signal for $x_c > x_r$ was not predicted asymptotically. It is shown in Figs. 2.9 and 2.11 that these effects do not cause a signicant difference between the numerical integration and the asymptotic approximation of the difference in the magnitudes of the total crack perturbed output voltage with that of a defect-free surface ($|\delta V| - |\delta V_o|$).

The strong ripples for $x_c < x_r$ in Fig. 2.10 indicate why the surface features stand out so vividly in acoustic images. This agrees with the observations of Ilett, *et al.* (1984). Also, the ripples for $x_c > x_r$ in both Figs. 2.9 and 2.11 are spaced approximately $\lambda_r/2$ apart in agreement with the observations made by Yamanaka and Enomoto (1982).

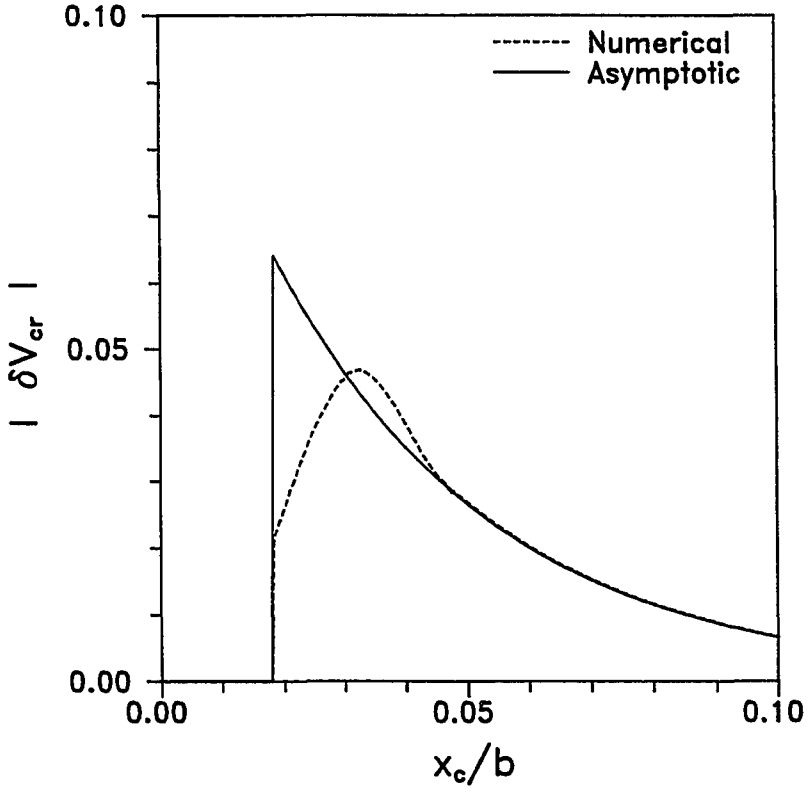

Fig. 2.8 The magnitude of that part of the acoustic signature caused by the presence of a surface-breaking crack located at x_c at a defocus of $z_s/\lambda_w = 5$ for fused quartz. The incident profile parameters are $n = 2$ and $a/b = 0.75$.

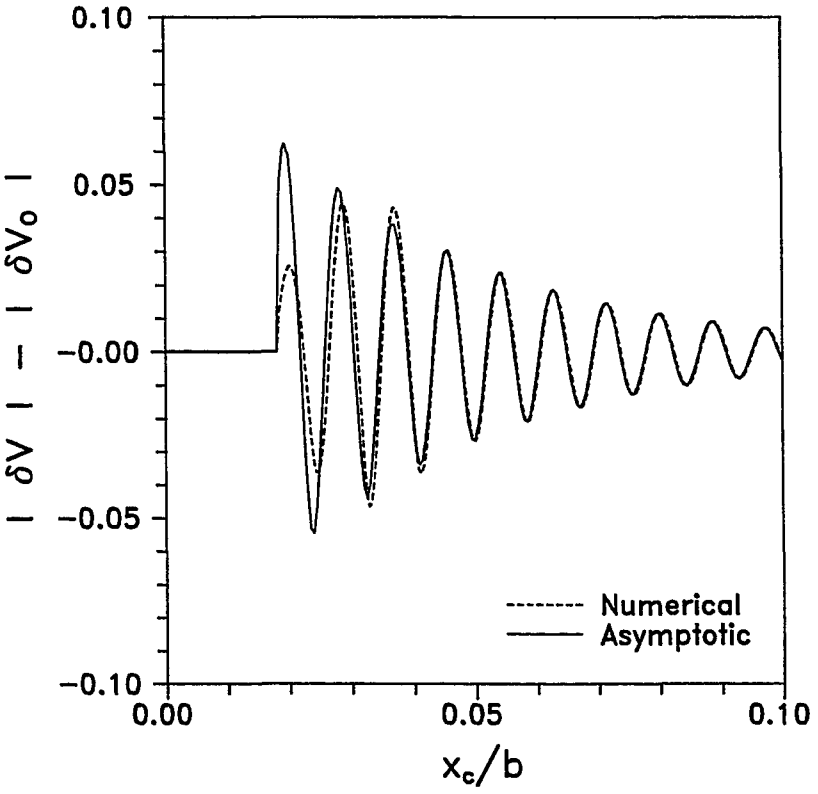

Fig. 2.9 The difference $|\delta V| - |\delta V_o|$ caused by the presence of a surface-breaking crack located at x_c at a defocus of $z_s/\lambda_w = 5$ for fused quartz. The incident profile parameters are $n = 2$ and $a/b = 0.75$.

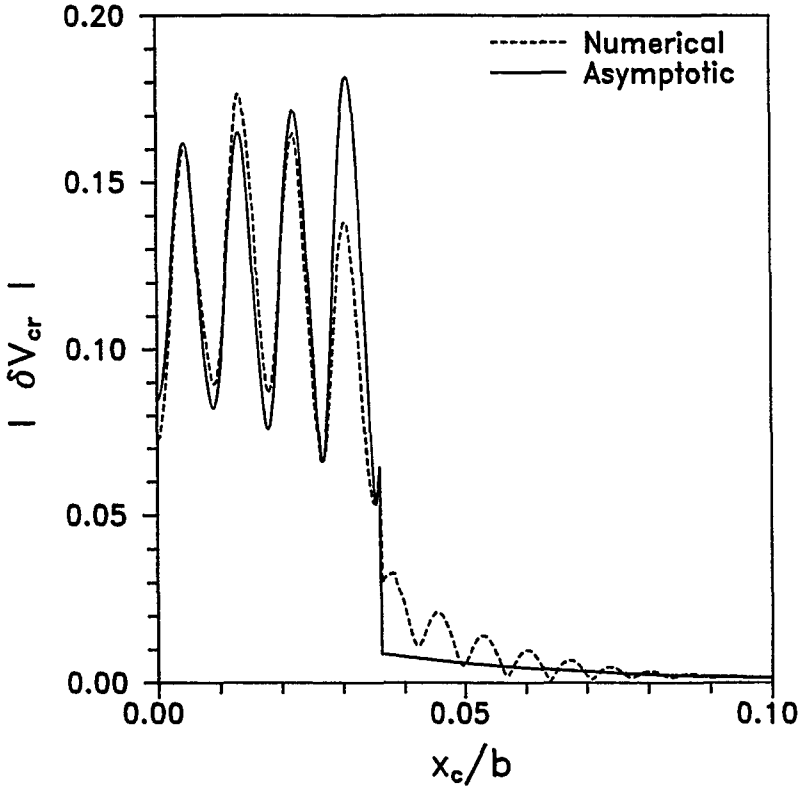

Fig. 2.10 The magnitude of that part of the acoustic signature caused by the presence of a surface-breaking crack located at x_c at a defocus of $z_s/\lambda_w = -10$ for fused quartz. The incident profile parameters are $n = 2$ and $a/b = 0.75$.

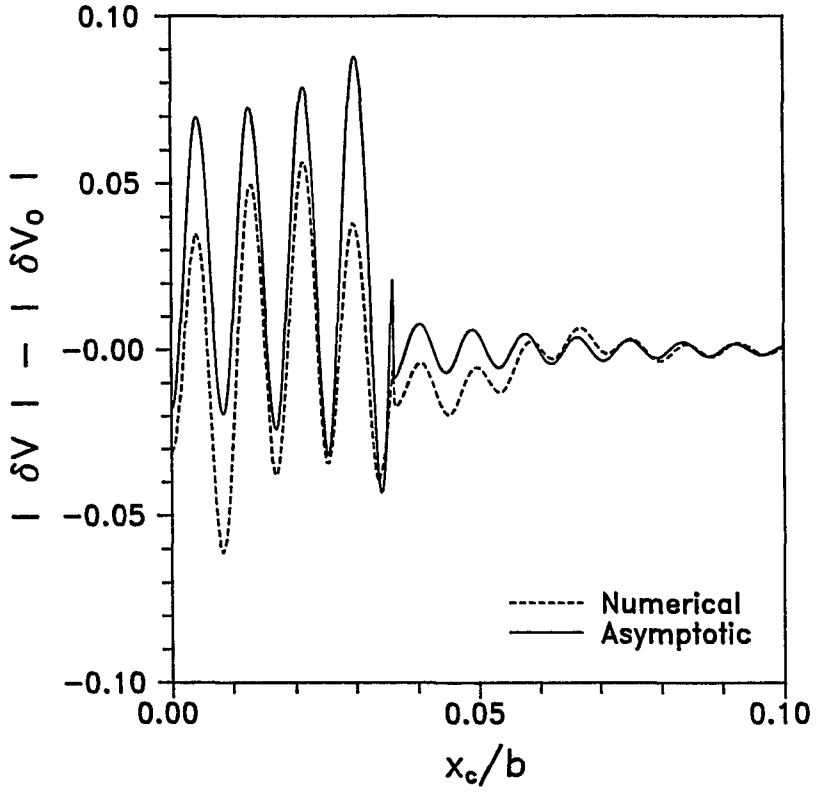

Fig. 2.11 The difference $|\delta V| - |\delta V_o|$ caused by the presence of a surface-breaking crack located at x_c at a defocus of $z_s/\lambda_w = -10$ for fused quartz. The incident profile parameters are $n = 2$ and $a/b = 0.75$.

2.6 A Quarter-Space

In the analytical developement of an approximate expression for the reflection coefficient of a surface-breaking crack, the reflection coefficient for a backscattered Rayleigh wave from a quarter-space is required (Achenbach, *et al.*, 1980). The strength of this backscattered surface wave and its corresponding reflection coefficient R_{qs} can be extracted from the acoustic signature δV_{qs} obtained by scanning horizontally at some defocus past the edge of the quarter-space. This calculation relies on the ability to measure the magnitude and phase accurately. With the magnitude and phase of the quarter-space's acoustic signature known, the term containing the backscattered reflection coefficient can be determined by vector subtraction.

2.6.1 The Scattered Wavefield

The wavefield scattered from the edge of a quarter-space is quite complex (Knopoff, 1969). This includes a backscattered leaky Rayleigh wave, a leaky Rayleigh wave which travels down the edge of the quarter-space plus diffracted body waves from the vertex of the quarter-space. There also is a diffracted wave in the fluid which is ignored since it is believed to be weak. All these signals are separated in time and some may not propagate towards the lens. Thus, only the wavefield of concern, the backscattered leaky Rayleigh wave, is collected by the aperture to interfere with the geometrically scattered wavefield from the interface. Hence, the scattered wavefield can be accurately approximated by just the geometrical and backscattered Rayleigh contributions.

First, considering that the geometrical focal point lies below the interface so that the incident wavefield is incoming, the total leaky Rayleigh wavefield is given in the following expression.

$$k^2\phi_{qs}^s = 2i\alpha_r E(\beta_r)\sqrt{2\pi}\exp(-ik\,|\,z-2z_s\,|\cos\beta_p)$$
$$\times\{u(x_e-x_r)u(x_r-x)\exp(-ikx\sin\beta_p)$$
$$+u(x_e+x_r)[u(x_r+x)-u(x-x_e)]\exp(ikx\sin\beta_p)$$
$$+u(x_e+x_r)u(x_e-x)R_{qs}\exp[ik(2x_e-x)\sin\beta_p]\}. \qquad (2.27)$$

Second, considering that the geometrical focal point lies above the interface so that the incident wavefield is outgoing, the leaky Rayleigh wavefield is

$$k^2\phi_{qs}^s = 2i\alpha_r E(\beta_r)\sqrt{2\pi}\exp(ik\,|\,z-2z_s\,|\cos\beta_p)$$
$$\times[u(x_e-x_r)\{u(x_e-x)R_{qs}\exp[ik(2x_e-x)\sin\beta_p]$$
$$+[u(x-x_r)-u(x-x_e)]\exp(ikx\sin\beta_p)\}$$
$$+u(x_e+x_r)u(-x-x_r)\exp(-ikx\sin\beta_p)]. \qquad (2.28)$$

Note that the edge of the quarter-space is given as $x=x_e$, which can be negative or positive, with the coordinate system placed at the incident wavefield's focal point. The Heaviside step functions $u(x)$ serve to partition the various regions of the surface. To obtain the total wavefield the geometric contribution is superimposed on Eqs. (2.27) and (2.28). Note that there is no reflected wave for positive x.

2.6.2 The Quarter-Space Acoustic Signature

Following the procedure outlined in earlier sections of this chapter, the quarter-space acoustic signature or output voltage δV_{qs} for the geometrical focal point below the surface is given by the following integrals evaluated along the interface.

$$\delta V_{qs}^{L} = C^{L}\int_{-\beta_a}^{\beta_e} E^2(\beta)R(\beta)\exp(-i2kbF\,|\,\bar{z}_s\,|\sec\beta)\,d\beta$$

$$-C^{L}\alpha_r E(\beta_r)\sqrt{2\pi k\,|\,z_s\,|}\exp\left(-i\frac{\pi}{4}\right)$$

$$\times\int_{-\beta_a}^{\beta_a} E(\beta_r)\sqrt{\sec\beta}\left(1+\frac{\cos\beta_r}{\cos\beta}\right)\exp(-ikbF\,|\,\bar{z}_s\,|\sec\beta)$$

$$\times\{u(x_e-x_r)u(x-x_e)\exp(-ikb\bar{x}\sin\beta_p)$$

$$+u(x_e+x_r)[u(x_r+x)-u(x-x_e)]\exp(ikb\bar{x}\sin\beta_p)$$

$$+u(x_e-x_r)u(x_e-x)R_{qs}\exp[ikb(2\bar{x}_e-\bar{x})\sin\beta_p]\}\,d\beta \qquad (2.29)$$

Note that $\beta_e > -\beta_a$ otherwise the output voltage is zero. Similiarly, δV_{qs}^{L} for the geometrical focal point above the surface is given by the following integrals evaluated along the interface.

$$\delta V_{qs}^{L} = -C^{L}\int_{-\beta_a}^{\beta_e} E^2(\beta)R(\beta)\exp(i2kbF\,|\,\bar{z}_s\,|\sec\beta)\,d\beta$$

$$+C^{L}\alpha_r E(\beta_r)\sqrt{2\pi k\,|\,z_s\,|}\exp\left(i\frac{\pi}{4}\right)$$

$$\times\int_{-\beta_a}^{\beta_a} E(\beta_r)\sqrt{\sec\beta}\left(1+\frac{\cos\beta_r}{\cos\beta}\right)\exp(ikbF\,|\,\bar{z}_s\,|\sec\beta)$$

$$\times[u(x_e-x_r)\{[u(x-x_r)-u(x-x_e)]\exp(ikb\bar{x}\sin\beta_p)$$

$$+u(x_e-x)R_{qs}\exp[ikb(2\bar{x}_e-\bar{x})\sin\beta_p]\}$$

$$+u(x_e+x_r)u(-x-x_r)\exp(-ikb\bar{x}\sin\beta_p)]\,d\beta \qquad (2.30)$$

In these expressions, $x = |\,z_s\,|\tan\beta$ and $x_r = |\,z_s\,|\tan\beta_r$ which denotes where the leaky Rayleigh wave is excited. Also, the corner position can be written as

$$\beta_e = \tan^{-1}\left(\frac{x_e}{|z_s|}\right) \tag{2.31}$$

with respect to the incident wavefield's focal point.

The exponential terms in the expressions for δV_{qs}^L, Eqs. (2.29) and (2.30), have been scaled in order that they may be asymptotically approximated. The geometric contribution has an endpoint, which describes the corner of the quarter-space, that can be equal to the saddlepoint; therefore, two forms of approximation are possible: non-uniform and uniform with respect to the saddlepoint approaching the endpoint of the integrals given in Eqs. (2.29) and (2.30). While it could be argued that using a non-uniform approximation to the scattered wavefield that excludes the effects of the vertex diffracted wavefield in an integral expression and then evaluating that integral uniformly is not consistent, it is believed that the uniform calculation of δV_{qs}^L gives considerable physical insight into the structure of the acoustic signature. Doing so uniformly gives, for the focal point below the interface,

$$\begin{aligned}
\delta V_{qs}^L = {} & \frac{R(0)E^2(0)}{\sqrt{k|z_s|}} Q\left[is_e \exp\left(-i\frac{\pi}{4}\right)\sqrt{2k|z_s|}\right] \exp\left(-i2k|z_s| - i\frac{\pi}{4}\right) \\
& + \frac{1}{4k|z_s|s_e} \exp\left[-i2k|z_s|(1+s_e^2) - i\frac{\pi}{2}\right] \\
& \times \left\{ 2R(\beta_e)E^2(\beta_e)\frac{|s_e|}{|\sin\beta_e|} - \sqrt{2}R(0)E^2(0)\right\} \\
& + 2\pi i C^L \alpha_r E^2(\beta_r)\exp(-i2k|z_s|\cos\beta_p) \\
& \times \{ u(x_e - x_r) + u(x_e + x_r)[1 - u(x_r - x_e) + R_{qs}\exp(i2kx_e\sin\beta_p)]\}
\end{aligned} \tag{2.32}$$

while for the focal point above the interface,

$$\delta V_{qs}^{L} = -\frac{R(0)E^2(0)}{\sqrt{k\,|z_s|}} Q\left[-is_e \exp\left(i\frac{\pi}{4}\right)\sqrt{2k\,|z_s|}\right] \exp\left(i2k\,|z_s| + i\frac{\pi}{4}\right)$$

$$+\frac{1}{4k\,|z_s|\,s_e} \exp\left[i2k\,|z_s|(1+s_e^2)+i\frac{\pi}{2}\right]$$

$$\times\left\{2R(\beta_e)E^2(\beta_e)\frac{|s_e|}{|\sin\beta_e|} - \sqrt{2}R(0)E^2(0)\right\}$$

$$+2\pi i C^L \alpha_r E^2(\beta_r)\exp(-i2k\,|z_s|\cos\beta_p)$$

$$\times u(x_e - x_r) R_{qs} \exp(i2kx_e \sin\beta_p)\,. \qquad (2.33)$$

The parameter s_e is defined as $s_e = \pm\sqrt{1-\sec\beta_e}$. The plus sign is used for $-\beta_e > 0$ and the negative on when $-\beta_e < 0$. The function Q in Eqs. (2.32) and (2.33) is the complementary error function with a complex argument. This can be written in terms of Fresnel integrals with real arguments (Felson and Marcuvitz, 1973) as shown below

$$Q\left[w\exp\left(\pm i\frac{\pi}{4}\right)\right] = \frac{1}{2}\sqrt{\pi} - \exp\left(\pm i\frac{\pi}{4}\right)\left[\overline{C}(w) - \exp\left(\pm i\frac{\pi}{2}\right)\overline{S}(w)\right] \qquad (2.34)$$

where the Fresnel integrals $\overline{C}$ and $\overline{S}$ are defined as

$$\overline{C}(w) = \int_0^w \cos t^2\, dt \qquad (2.35)$$

and

$$\overline{S}(w) = \int_0^w \sin t^2\, dt\,. \qquad (2.36)$$

These two uniform asymptotic expansions for δV_{qs}^{L} can be compared to non-uniform asymptotic approximations of the geometric contribution. For the focal point below the interface, one non-uniformly obtains

$$\begin{aligned}\delta V_{qs}^{L} = & R(0)E^{2}(0)\sqrt{\frac{\pi}{k\,|z_s|}}\exp\left(-i2k\,|z_s|-i\frac{\pi}{4}\right)u(\beta_e) \\ & +R(\beta_e)E^{2}(\beta_e)\frac{\exp(-i2k\,|z_s|\,s_e^{2})}{2ik\,|z_s|\sin\beta_e} \\ & +2\pi i C^{L}\alpha_r E^{2}(\beta_r)\exp(-i2k\,|z_s|\cos\beta_p) \\ & \quad\times\{u(x_e-x_r)+u(x_e+x_r)[1-u(x_r-x_e)+R_{qs}\exp(i2kx_e\sin\beta_p)]\}\end{aligned} \tag{2.37}$$

and similiarly, for the focal point above the interface

$$\begin{aligned}\delta V_{qs}^{L} = & -R(0)E^{2}(0)\sqrt{\frac{\pi}{k\,|z_s|}}\exp\left(i2k\,|z_s|+i\frac{\pi}{4}\right)u(\beta_e) \\ & -R(\beta_e)E^{2}(\beta_e)\frac{\exp(i2k\,|z_s|\,s_e^{2})}{2ik\,|z_s|\sin\beta_e} \\ & +2\pi i C^{L}\alpha_r E^{2}(\beta_r)\exp(-i2k\,|z_s|\cos\beta_p) \\ & \quad\times u(x_e-x_r)R_{qs}\exp(i2kx_e\sin\beta_p).\end{aligned} \tag{2.38}$$

The non-uniform and uniform asymptotic approximations for the quarter-space acoustic signature δV_{qs}^{L} for fused quartz are shown in Fig. 2.12 for a defocus of $z_s/\lambda_w=-10$ and in Fig. 2.13 for a defocus of $z_s/\lambda_w=5$. In comparing the two asymptotic results, good agreement occurs when the edge position x_e is a certain distance from the origin on the interface, which is given as

$$|x_e| \gg \sqrt{\left(|z_s|+\frac{1}{k}\right)^{2}-|z_s|^{2}}\quad . \tag{2.39}$$

For the ability to extract the reflection coefficient of the backscattered leaky Rayleigh wave, the non-uniform result can be used accurately as long as the constraint given in Eq. (2.39) is satisfied.

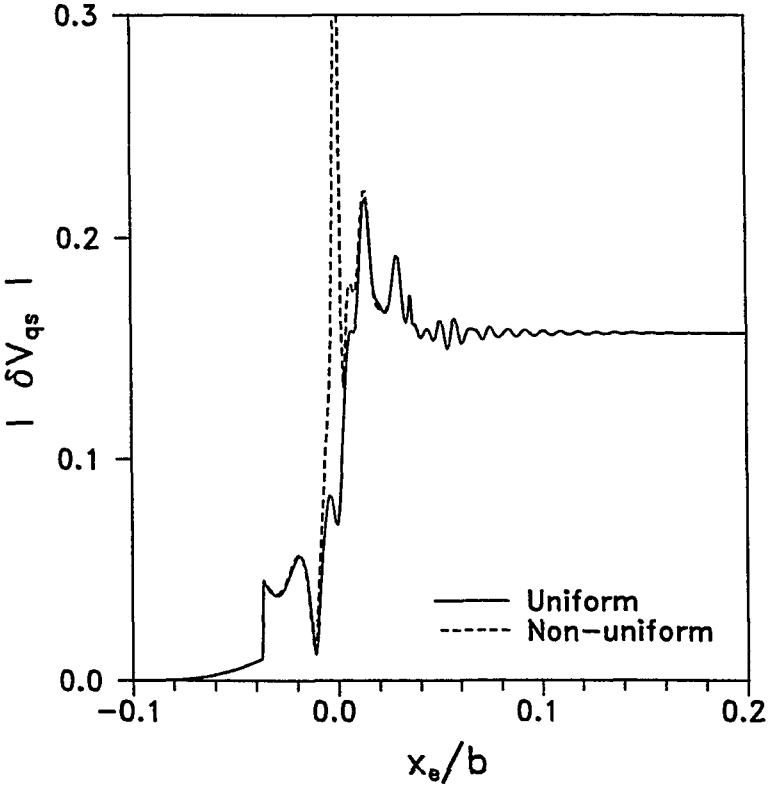

Fig. 2.12 The magnitude of the acoustic signature caused by the presence of a quarter-space located at x_e at a defocus of $z_s/\lambda_w = -10$ for fused quartz.

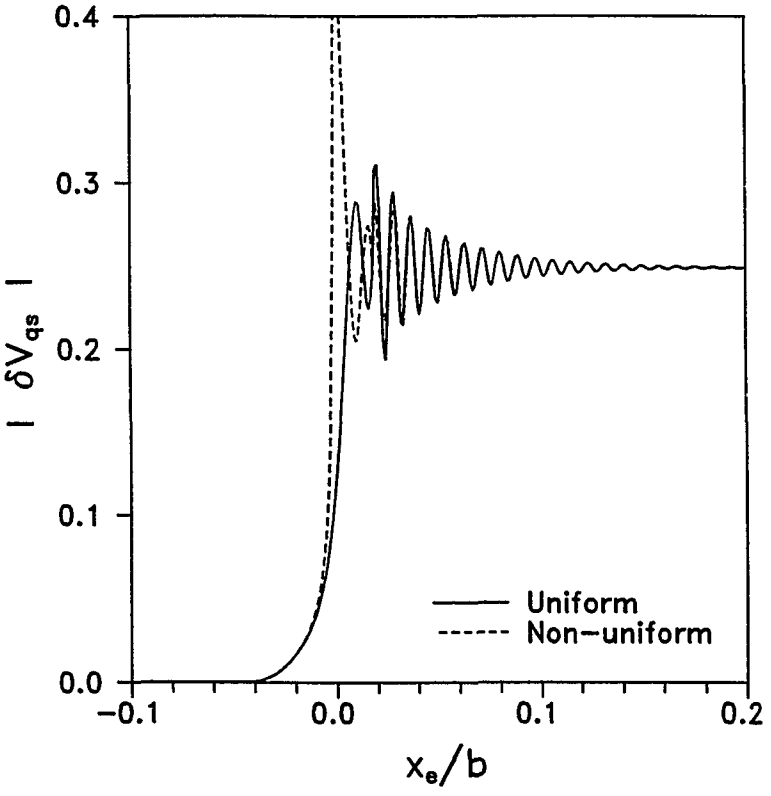

Fig. 2.13 The magnitude of the acoustic signature caused by the presence of a quarter-space located at x_e at a defocus of $z_s/\lambda_w = 5$ for fused quartz.

CHAPTER 3

Point Focus Microscope

3.1 Introduction

In this chapter the study of the acoustic signature of a surface containing a surface-breaking crack (Rebinsky and Harris, 1991) is continued in this instance using a point focus scanning acoustic microscope. An estimate of the voltage or the acoustic signature measured using a point focus lens is obtained, and then this result is compared to that for a line focus lens. The point focus scanning acoustic microscope produces an incident axisymmetric focused beam which excites a geometrically reflected beam and a leaky Rayleigh wave. For a point focus microscope, the leaky Rayleigh wave can focus to a point on the interface. The interaction of these two signals, geometric and Rayleigh, produces an interference pattern in the output voltage. The purpose of this chapter is to explore how the point focus microscope can be used to acquire quantitative information about surface-breaking cracks from the acoustic signature. Moreover, a comparison with the line focus device will be made to understand their different measurement capabilities.

Because a leaky Rayleigh wave contributes significantly to the acoustic signature, the scanning acoustic microscope is particularly sensitive to vertical discontinuities such as surface-breaking cracks. In Chap. 1, some literature was reviewed describing much of the research done to measure the acoustic signature of a surface-breaking crack as well as that done to study the scattering of Rayleigh waves from such a crack. It is of interest to note that previous researchers (Rowe, *et al.* 1986; Briggs *et al.*, 1990) have compared two dimensional calculations of the acoustic signature for a surface-breaking crack with measurements made using a point focus scanning acoustic microscope. Although there is qualitative agreement, there are

discrepancies when three dimensional experimental results are studied with two dimensional theory. From our asymptotic expressions of the crack perturbed acoustic signature, it is possible to explain these occurances.

3.2 The Incident Wavefield

To construct the incident axisymmetric focused wavefield, the Debye approximation (Stamnes, 1986, pp. 243-281 and 455-481) is used. The geometry is shown in Fig. 2.1. The incident wavefield ϕ^i is given by

$$k^2\phi^i = -\frac{1}{2}\int_{-\beta_a}^{\beta_a} G(\beta)\sin\beta \begin{matrix} H_0^{(1)} \\ H_0^{(2)} \end{matrix}(2\pi FN\bar{\rho}\sin\beta)\exp(\pm i2\pi F^2N\,|\,\bar{z}\,|\cos\beta)\,d\beta\,. \tag{3.1}$$

The functions $H_0^{(1)}, H_0^{(2)}$ indicate the zero order Hankel functions of the first and the second kind. The minus sign and $H_0^{(2)}$ indicate a disturbance incoming to the focal plane, and the plus sign and $H_0^{(1)}$ denote one which is outgoing. The coordinate $\bar{\rho} = \rho/b$, b is the half-width of the lens' aperture (Fig. 2.1), and k is the wave number in the fluid. The focal length f is defined in Fig. 2.1 and $\bar{z} = z/f$. The amplitude function $G(\beta)$ and the (possibly complex) angle β_a remain to be determined. In the focal plane, $\phi^i(x,0)$ is the Hankel transform of $G(\beta)$.

Recall from the previous chapter that the two parameters characterizing the focused beam are the Fresnel number N and the F-number F given by Eqs. (2.2) and (2.3). Recall that the cases when $F = O(1)$ and N is large are of interest. Thus, $kb = 2\pi FN$ is large. Accordingly, the integral in Eq. (3.1) is readily approximated asymptotically, giving

$$\phi^i = \pm i\frac{G(\Theta)}{k^2}\frac{\exp(\pm ikR)}{kR} \tag{3.2}$$

where $R=\sqrt{\rho^2+z^2}$ and $\rho=|z|\tan\Theta$. Also, $0\le\Theta\le\pi/2$.

To determine $G(\beta)$ and β_a, it is demanded that ϕ^i asymptotically match a given ϕ^i at $z=-f$, the lens' aperture. It is assumed that edge-diffracted waves are not strongly excited. Accordingly, the following aperture distribution is proposed for $|\rho|\le b$:

$$\phi^i=\frac{B}{k^2}\exp\left[-\left(\frac{b}{a}\frac{\rho}{b}\right)^{2n}\right]\frac{\exp(-ikR_o)}{kR_o} \tag{3.3}$$

where B is an amplitude constant, a is a parameter that measures how fully the beam fills the aperture and n is an integer greater than or equal to unity that determines how abruptly the distribution falls off at a. The distance $R_o=\sqrt{\rho^2+f^2}$. If b is allowed to go to infinity then the distribution goes to zero at the edges, while if b is finite, provided $a/b<1$, the magnitude is small at b. Moreover, provided n is not too large, the magnitude of ϕ^i does not fall off abruptly at $\rho=a$.

Equating Eq. (3.2) to Eq. (3.3) gives

$$G(\beta)=B\exp\left[-\left(F\frac{b}{a}\tan\beta\right)^{2n}\right]\exp\left(i\frac{\pi}{2}\right). \tag{3.4}$$

As with the line focus microscope, the angle $\beta_a=\tan^{-1}F$ defines the aperture opening. Figure 3.1 shows transverse profiles for the incident axisymmetric acoustic beam radiated into the fluid at the plane of the lens' aperture, for n = 1, 2 and 4, and a/b = 0.50, 0.75 and 0.85, respectively. The frequency of operation is 225 MHz. The fluid is water with a density of 998 kg/m^3 and a wavespeed of 1480 m/s. The Fresnel number equals 178 and the F-number equals 0.753. These are the same microscope parameters used in Chap.2 for the line focus lens. Note that in all cases

the magnitude of the incident wavefield is not large at the edge of the lens' aperture.

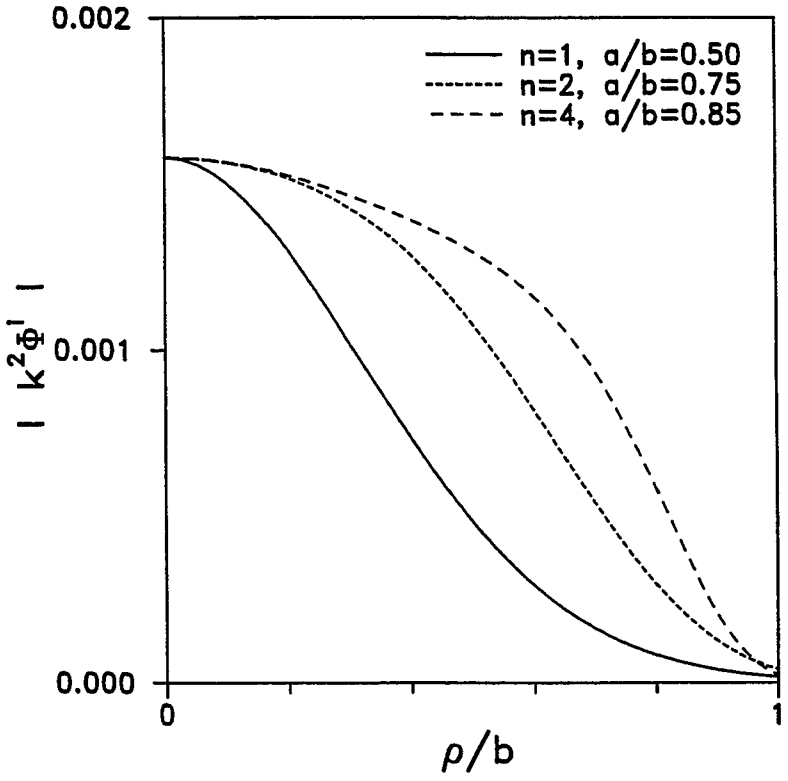

Fig. 3.1 Transverse profiles along the lens' aperture of the axisymmetric acoustic beam radiated into the fluid.

3.3 The Scattered Wavefield for a Defect-Free Surface

Figure 2.1 also shows the geometry for the scattered wavefield. Note that $z = z_S$ gives the position of the interface between the solid and the coupling fluid relative to the geometrical focal point. Because the incident wavefield is expressed as an angular spectrum, the scattered wavefield ϕ^s is readily constructed giving

$$k^2\phi^s = -\frac{1}{2}\int_{-\beta_a}^{\beta_a} G(\beta)R(\beta)\sin\beta \frac{H_0^{(1)}}{H_0^{(2)}}(kb\bar{\rho}\sin\beta)\exp(\pm ikbF\,|\bar{z}-2\bar{z}_s|\cos\beta)\,d\beta\,. \tag{3.5}$$

The minus sign and $H_0^{(2)}$ indicate a disturbance incoming to the reflected focal plane, at $z = z_S$, and the plus sign and $H_0^{(1)}$ indicate one which is outgoing. The term $R(\beta)$ is the plane-wave reflection coefficient for the displacement potential for a fluid-solid interface. As discussed in section 2.2, it is the leaky Rayleigh waves in this problem that are most strongly excited, provided β_a is sufficiently large. The structure of $R(\beta)$ and of the complex β plane is discussed further in Appendix A.

The basic physical components of Eq. (3.5) are exhibited by a non-uniform asymptotic approximation. When the focal point lies below the surface of the specimen, the wavefield is

$$\begin{aligned} k^2\phi^s = &-i\,G(\theta)R(\theta)\frac{\exp(-ikr)}{kr} \\ &+2\pi\alpha_r\sin\beta_r\,G(\beta_r)\exp(-ikr\cos\theta\cos\beta_p) \\ &\times[H_0^{(1)}(kr\sin\theta\sin\beta_p)+u(\beta_r-\theta)H_0^{(2)}(kr\sin\theta\sin\beta_p)]\,. \end{aligned} \tag{3.6}$$

Note that the leaky Rayleigh contribution is proportional to the zero order Bessel function $J_0(w)$ when $\theta < \beta_r$. In contrast, recall that the diffracted wavefield from a circular aperture is described by $J_1(w)/w$. When the focal point lies above the surface of the specimen, the wavefield is

$$k^2\phi^s = i\,G(\theta)R(\theta)\frac{\exp(ikr)}{kr} + 2\pi\alpha_r \sin\beta_r G(\beta_r)\exp(-ikr\cos\theta\cos\beta_p) \times u(\theta-\beta_r)H_0^{(1)}(kr\sin\theta\sin\beta_p)\,. \tag{3.7}$$

The coordinates r and θ are given by

$$\rho = r\sin\theta \tag{3.8}$$

where $\rho^2 = x^2+y^2$ and

$$|z-2z_s| = r\cos\theta\,. \tag{3.9}$$

In this axisymmetric problem, the domains of θ and r are $0 \le \theta \le \pi/2$ and $r \ge 0$ respectively. The Rayleigh pole is given by $\beta_p = \beta_r + i\alpha_r$. The α_r indicates that the wave is leaky, and does not indicate an attenuation caused by viscosity or other loss mechanism in the fluid or solid. The residue of the reflection coefficient can be approximated by $\pm 2i\,\alpha_r$ at $\beta = \pm\beta_p$ as stated by Eq. (2.12) in section 2.2. Because α_r is small, β_p has been approximated by β_r in the amplitude terms. The function $u(x)$ is the Heaviside function. The first terms in Eqs. (3.6) and (3.7) are the geometrical ones, while the second terms represent the leaky Rayleigh waves. Note that in order to excite the Rayleigh wave strongly, β_a must be greater than β_r.

Figure 3.2 shows the transverse profile for the axisymmetric scattered wavefield, calculated using Eq. (3.7), at the plane of the lens' aperture where the geometrical component has undergone sufficient geometrical decay so that the presence of the Rayleigh wave is clear.

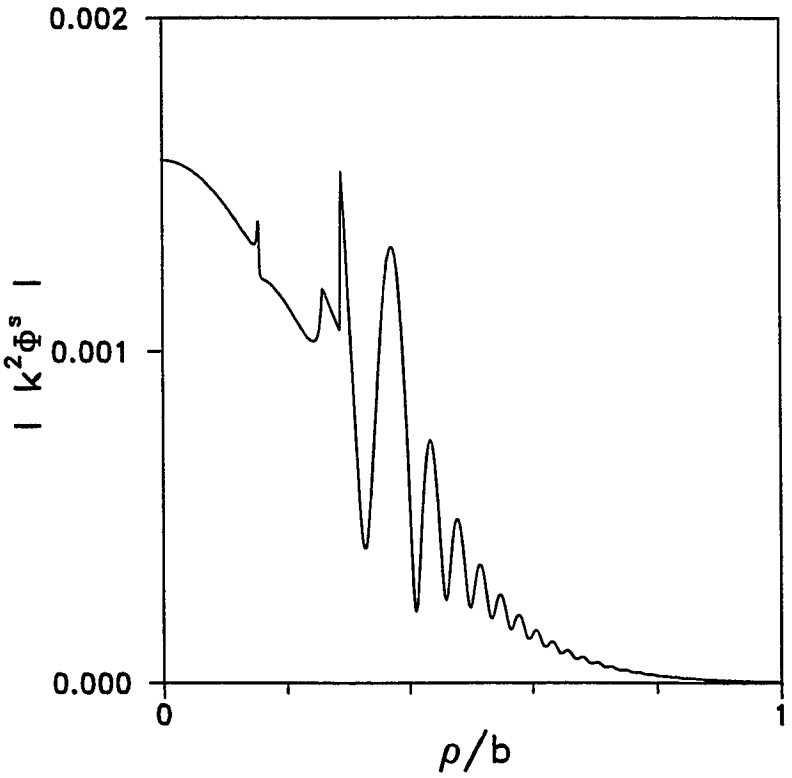

Fig. 3.2 Transverse profile along the lens' aperture of the axisymmetric scattered wavefield for fused quartz at a defocus of $z_s/\lambda_w = -10$. The incident profile parameters are $n = 1$ and $a/b = 0.50$.

The solid is fused quartz, whose density, longitudinal wavespeed and transverse wavespeed are 2200 kg/m^3, 5960 m/s and 3760 m/s, respectively. The remaining parameters are those used in the previous figure and the incident beam profile is described by a Gaussian beam where $n = 1$ and $a/b = 0.5$. This beam profile will be used throughout the rest of this chapter although it is different than the parameters used in the previous chapter on the line focus

microscope. This choice of parmaters maximizes the amplitude of oscillation of the acoustic signatures to be shown later in this chapter. Large oscillations on the scattered beam profile are observed in Fig. 3.2 when compared to the incident beam profile shown in Fig. 3.1 which indicate the strong influence of the leaky Rayleigh wave on the signal collected by the lens.

3.4 The Acoustic Signature for a Defect-Free Surface

The acoustic signature is calculated by using the asymptotic expressions for ϕ^i and ϕ^s, and evaluating Eq. (1.1) along a suitable surface S. Taking S to be the interface is satisfactory except for values of z_s quite close to zero. The defect-free acoustic signature is

$$\begin{aligned}\delta V_o^P = &-2iC^P \int_0^{\beta_a} G^2(\beta) R(\beta) \sin\beta \exp(-i2kbF\,|\bar{z}_s|\sec\beta)\, d\beta \\ &+ 2\pi k\,|z_s|\, C^P \alpha_r \sin\beta_r\, G(\beta_r) \exp(-ikbF\,|\bar{z}_s|\cos\beta_p) \\ &\times \int_0^{\beta_a} G(\beta)\tan\beta\left(1+\frac{\cos\beta_r}{\cos\beta}\right)\exp(-ikbF\,|\bar{z}_s|\sec\beta) \\ &\times \{H_0^{(1)}(kbF\,|\bar{z}_s|\tan\beta\sin\beta_p) + u(\beta_r-\beta) H_0^{(2)}(kbF\,|\bar{z}_s|\tan\beta\sin\beta_p)\}\, d\beta \end{aligned} \tag{3.10}$$

when the focal point is below the interface and

$$\begin{aligned}\delta V_o^P = &-2iC^P \int_0^{\beta_a} G^2(\beta) R(\beta) \sin\beta \exp(+i2kbF\,|\bar{z}_s|\sec\beta)\, d\beta \\ &- 2\pi k\,|z_s|\, C^P \alpha_r \sin\beta_r\, G(\beta_r) \exp(+ikbF\,|\bar{z}_s|\cos\beta_p) \\ &\times \int_{\beta_r}^{\beta_a} G(\beta)\tan\beta\left(1+\frac{\cos\beta_r}{\cos\beta}\right)\exp(+ikbF\,|\bar{z}_s|\sec\beta) \\ &\times H_0^{(1)}(kbF\,|\bar{z}_s|\tan\beta\sin\beta_p)\, d\beta \end{aligned} \tag{3.11}$$

when the focal point is above the interface. The subscript o indicates that the surface is unbroken. The superscript P denotes a point focus microscope. Note that the new normalizing constant C^P is proportional to the old one $\tilde{C}$ given in Eq. (1.2).

$$\frac{1}{C^P} = 2i \int_0^{\beta_a} G(\beta) G^*(\beta) \sin\beta \, d\beta \tag{3.12}$$

Further, these integrals describing the acoustic signature using a point focus lens are readily approximated asymptotically, giving

$$\delta V_o^P = -C^P G^2(0) R(0) \frac{\exp(\pm 2ik \mid z_s \mid)}{k \mid z_s \mid}$$

$$- u(-z_s) C^P G^2(\beta_r) 8\pi i \, \alpha_r \sin\beta_r \exp(-2ik \mid z_s \mid \cos\beta_p) . \tag{3.13}$$

For positive defocus $z_s > 0$, the pole term in Eq. (3.11) has been ignored. These terms will be small, because of the secant in the exponential in the geometric term, for $kbF \mid \bar{z}_s \mid$ of moderate size and an α_r which is not very small. For α_r small, the original asymptotic results are not accurate near β_p. Thus Eq. (3.11) cannot be expected to give accurate results in this region.

It is relatively easy to calculate the asymptotic contribution from the endpoint, provided β_a is not close to β_r. That term is $O(1/kb)$, which is identical in order to the geometrical term of the point focus lens, and its strength is proportional to $G(\beta_a)$ which is chosen to be small so that it can be ignored.

One can repeat this calculation using the plane of the lens' aperture as the surface S. Interestingly, both it and Eqs. (3.10) and (3.11) yield Eq. (3.13) when they are evaluated asymptotically subject to the previous discussion of Eq. (3.11).

Recall that both the incident and the scattered wavefields are expressed as Hankel transforms. If these expressions are substituted directly into Eq. (1.1) where advantage has been taken of Parseval's relation, the expression for the change in voltage can be expressed as

$$\delta V_o^P = 2iC^P \int_0^{\beta_a} G^2(\beta) R(\beta) \sin\beta \exp(\pm 2ikbF \mid \bar{z}_s \mid \cos\beta) d\beta . \tag{3.14}$$

The plus sign is used when the focal point is above, and the minus sign is used when it is below the interface. In addition to being quite simple, Eq. (3.14) contains no reference to the contour of integration S. Of considerable interest is the fact that this spectral result for the acoustic signature also yields Eq.(3.13) when asymptotically evaluated.

Figure 3.3 shows a plot of $\mid \delta V_o \mid$ against z_s/λ_w, where λ_w is the wavelength in water, calculated in several ways. The solid line is calculated using the asymptotic result Eq. (3.13), the short dashed line using the spectral expression Eq. (3.14), and the longer dashed line using the integration over the interface, Eqs. (3.10) and (3.11). The solid is fused quartz. The values of the various microscope parameters are those used previously. The curves do not agree precisely, but their agreement is nevertheless remarkable. The oscillations in the numerical results for positive defocus are a consequence of our earlier remark concerning Eq. (3.11). All the expressions exhibit the basic physical mechanisms that contribute to the acoustic signature. Note that when the focal point is below the interface the signals caused by the geometric and the leaky Rayleigh wave interfere, giving an interference pattern as z_s is changed. The distance between the peaks $\Delta \mid z_s \mid$ is described by Eq. (2.14).

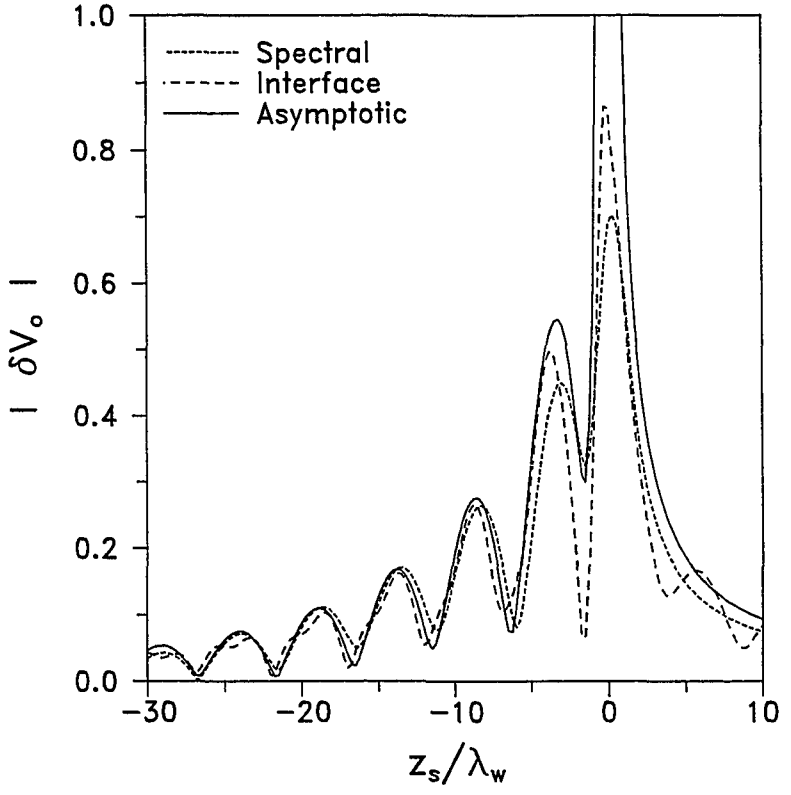

Fig. 3.3 The acoustic signature for fused quartz calculated in three distinct ways.

In Fig. 3.4, the dependence of the asymptotic acoustic signature on the profile of the incident acoustic beam is shown for the following set of parameters: $n = 1$, 2 and 4, and a/b = 0.50, 0.75 and 0.85, respectively. The shape of the curves remains the same although the amplitude of the oscillations for negative defocus is diminished as the incident beam profile becomes more uniform.

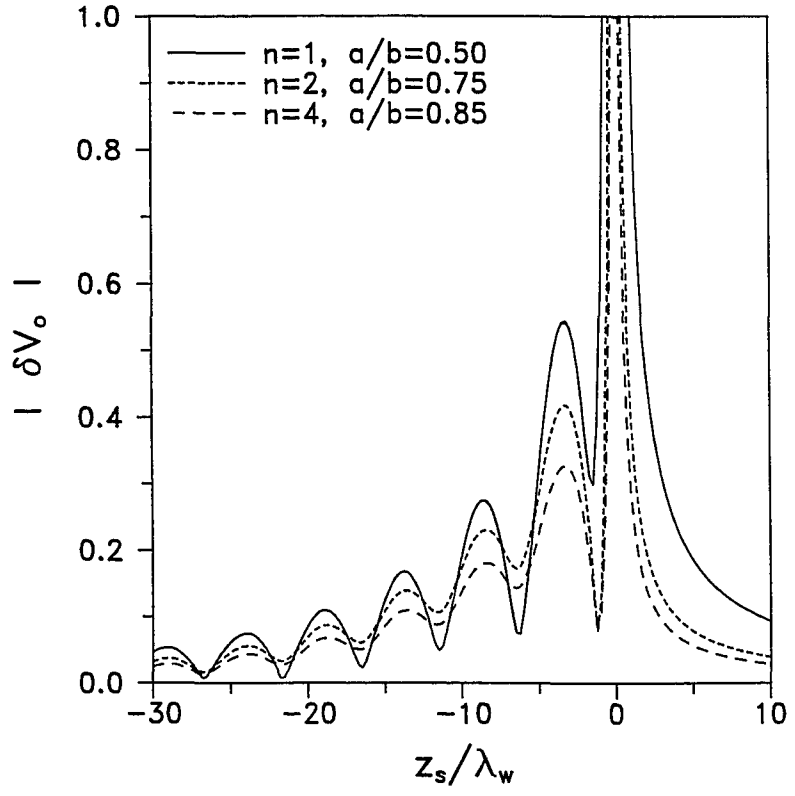

Fig. 3.4 The dependence of the acoustic signature for fused quartz on the incident beam profile.

Because both point focus and line focus lenses are available, it is useful to compare the acoustic signatures measured using each lens. Comparison of the spectral results is more convenient. Recall from Chap. 2 that the voltage change measured using a line focus lens, δV_0^L is given in Eq. (2.12) as

$$\delta V_o^L = -2iC^L \int_0^{\beta_a} E^2(\beta) R(\beta) \exp(\pm 2ikbF \mid \bar{z}_s \mid \cos\beta) d\beta . \tag{3.15}$$

The asymptotic approximation of Eq. (3.15) is Eq. (2.14)

$$\delta V_o^L = -C^L E^2(0) R(0) \sqrt{\frac{\pi}{k \mid z_s \mid}} \exp(\pm 2ik \mid z_s \mid) \left[\pm \exp\left(\pm i \frac{\pi}{4} \right) \right]$$
$$+ u(-z_s) C^L E^2(\beta_r) 8\pi i \alpha_r \exp(-2ik \mid z_s \mid \cos\beta_p) \tag{3.16}$$

which is repeated here for convenience.

First, note that Eqs. (3.14) and (3.15) have the same general form except that the integrand of Eq. (3.14) contains $\sin\beta$. Thus the geometrical term in (3.13) for the point focus lens has an $O(1/k \mid z_s \mid)$ dependence, while that in Eq. (3.16) for the line focus lens has an $O(1/\sqrt{k \mid z_s \mid})$ dependence. But what is remarkable result is that the leaky Rayleigh wave contribution in both cases is of the same order of magnitude. The leaky Rayleigh term for the point focus lens is only decreased in magnitude by $\sin\beta_r = c/c_r$. Figure 3.5 compares the spectral output voltages for fused quartz calculated by numerical integration of $\mid \delta V_o^P \mid$ given by Eq. (3.14), the solid line, with $\mid \delta V_o^L \mid$ given by Eq. (3.15), the dashed line. The Fresnel number, F-number and incident profile parameters are identical for both calculations.

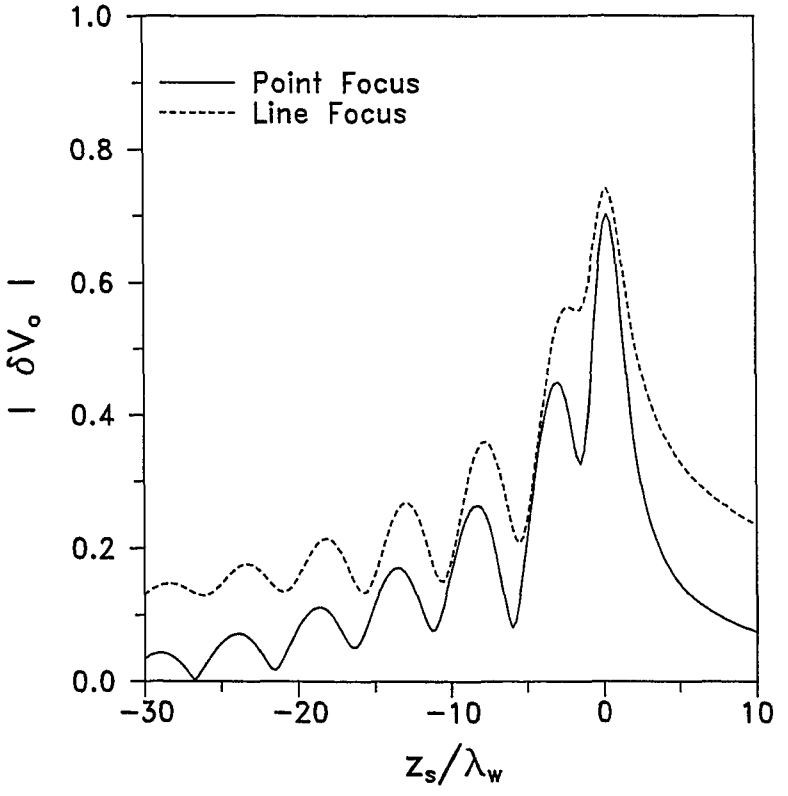

Fig. 3.5 A comparison of the acoustic signatures using line focus and point focus lenses for fused quartz. The incident profile parameters are $n = 1$ and $a/b = 0.50$.

The interference patterns have the same basic form with any differences being caused by the order of their respective geometrical contributions. Somekh, *et al.* (1985) and, more recently, Briggs, *et al.* (1990) have compared their three dimensional experimental data with a two dimensional theory. They obtained good agreement when the defocus of the two dimensional theory was slightly shifted. This shift between the results for the two lenses, point focus and line focus, can also be observed in Fig. 3.5.

3.5 A Surface with a Surface-Breaking Crack

When the focused acoustic beam is scattered from a surface broken by a crack many scattered disturbances are excited as discussed in section 2.5 concerning the line focus microscope. From that discussion, the leaky Rayleigh waves are expected to interact very strongly with the crack because they strike it broadside. An examination of the work cited in Chap. 1 suggests that the dominant wave processes of concern are those of reflection and transmission. Thus, it is assumed that the crack can be characterized by reflection and transmission coefficients which are functions of the angle of incidence of the leaky Rayleigh wave striking the surface-breaking crack.

3.5.1 The Scattered Wavefield

The wavefield scattered from the broken surface, making the approximations just described, consists of Eqs. (3.6) and (3.7) plus the terms that take into account the reflection and transmission of the obliquely incident leaky Rayleigh waves by the surface-breaking crack. Let the crack be located at $x = x_c$, where x_c is taken to be positive (Fig. 2.1). Further, let the reflection and transmission coefficients be the complex parameters $R_r(\gamma)$ and $T_r(\gamma)$ respectively, where γ indicates the angle of incidence of the Rayleigh wave with respect to the normal to the crack face. For a vertical surface-breaking crack, they are functions of d/λ_r, where d is the crack depth and λ_r is the Rayleigh wavelength, as well as the various material properties as stated in section 2.5.1. Lastly, let the radius $x_r = | z_s | \tan \beta_r$ indicate the position on the surface where the incident Rayleigh waves are excited.

First, consider that the geometrical focal point lies below the interface so that the incident wavefield is incoming. The scattered leaky Rayleigh waves are given by the following expression.

$$
\begin{aligned}
k^2\phi^s_{cr} = {} & 2\alpha_r \sin\beta_r G(\beta_r)\exp(-ik\,|\,z-2z_s\,|\cos\beta_p) \\
& \times\{u(x_c-x)\int_{-\frac{\pi}{2}}^{\frac{\pi}{2}} R_r(\gamma)\exp\{ik\sin\beta_p[(2x_c-x)\cos\gamma+y\sin\gamma]\}\,d\gamma \\
& + u(x-x_c)\int_{-\frac{\pi}{2}}^{\frac{\pi}{2}} [T_r(\gamma)-1]\exp[ik\sin\beta_p(x\cos\gamma+y\sin\gamma)]\,d\gamma \\
& + u(x_r-x_c)u(x-x_c)u\left(|2-\frac{x}{x_c}|-|\frac{y}{\sqrt{x_r^2-x_c^2}}|\right) \\
& \quad \times\int_{-\frac{\pi}{2}}^{\frac{\pi}{2}} R_r(\gamma)\exp\{-ik\sin\beta_p[(2x_c-x)\cos\gamma+y\sin\gamma]\}\,d\gamma \\
& + u(x_r-x_c)u(x-x_c)u\left(|\frac{x}{x_c}|-|\frac{y}{\sqrt{x_r^2-x_c^2}}|\right) \\
& \quad \times\int_{-\frac{\pi}{2}}^{\frac{\pi}{2}} [T_r(\gamma)-1]\exp[-ik\sin\beta_p(x\cos\gamma+y\sin\gamma)]\,d\gamma\,\}
\end{aligned}
\tag{3.17}
$$

In the third term for $x > 2x_c$ and in the fourth term for $x < 0$, the outgoing wave is obtained by performing the change of variable $\gamma = -\gamma$. The crack scattered wavefield for this case is traced as rays on the interface in Fig. 3.6.

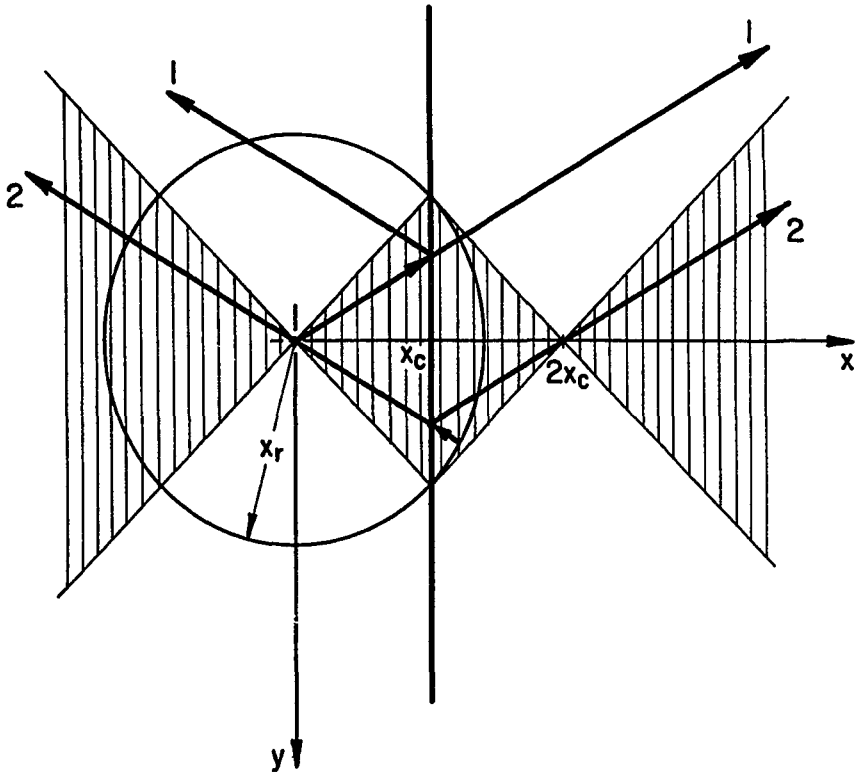

Fig. 3.6 A ray tracing of the crack scattered wavefield on the interface when the geometrical focal point lies below the interface. 1 shows a typical set of rays coming from those portions of the Rayleigh excitation circle to the left of the crack. 2 shows a typical set of rays coming from the right of the crack. The shaded regions are those reached by the rays coming from the right portion of the Rayleigh excitation circle.

Secondly, consider that the geometrical focal point lies above the interface so that the incident wavefield is outgoing. The scattered leaky Rayleigh waves for $x_r < x_c$ (Fig. 3.7) are

$$k^2\phi^s_{cr} = 2\alpha_r \sin\beta_r\, G(\beta_r) \exp(ik\,|z-2z_s|\cos\beta_p)\, u(x_c-x_r)$$

$$\times\{u(x_c-x)\int_{-\frac{\pi}{2}}^{\frac{\pi}{2}} R_r(\gamma)\exp\{ik\sin\beta_p[(2x_c-x)\cos\gamma+y\sin\gamma]\}\,d\gamma$$

$$+u(x-x_c)\int_{-\frac{\pi}{2}}^{\frac{\pi}{2}}[T_r(\gamma)-1]\exp[ik\sin\beta_p(x\cos\gamma+y\sin\gamma)]\,d\gamma\} \qquad (3.18)$$

and

$$k^2\phi^s_{cr} = 2\alpha_r \sin\beta_r\, G(\beta_r) \exp(ik\,|z-2z_s|\cos\beta_p)\, u(x_r-x_c)$$

$$\times\{u(x_c-x)\,u\left(\left|\frac{y}{\sqrt{x_r^2-x_c^2}}\right|-\left|2-\frac{x}{x_c}\right|\right)$$

$$\times\int_{-\frac{\pi}{2}}^{\frac{\pi}{2}} R_r(\gamma)\exp\{ik\sin\beta_p[(2x_c-x)\cos\gamma+y\sin\gamma]\}\,d\gamma$$

$$+u(x-x_c)\,u\left(\left|\frac{y}{\sqrt{x_r^2-x_c^2}}\right|-\left|\frac{x}{x_c}\right|\right)$$

$$\times\int_{-\frac{\pi}{2}}^{\frac{\pi}{2}}[T_r(\gamma)-1]\exp[ik\sin\beta_p(x\cos\gamma+y\sin\gamma)]\,d\gamma\} \qquad (3.19)$$

for $x_r > x_c$ (Fig. 3.8). These crack scattered leaky Rayleigh wavefields are constructed as follows. The Hankel functions in Eqs. (3.6) and (3.7) are written using the Sommerfeld integral representations. These representations express the Hankel functions as an angular spectrum of plane waves containing both propagating and evanescent components. The evanescent portion is

dropped. That is,

$$H_0^{(1)} \rightarrow \frac{1}{\pi}\int_{-\frac{\pi}{2}}^{\frac{\pi}{2}} \exp(iw\cos\gamma)\,d\gamma \tag{3.20}$$

and

$$H_0^{(2)} \rightarrow \frac{1}{\pi}\int_{-\frac{\pi}{2}}^{\frac{\pi}{2}} \exp(-iw\cos\gamma)\,d\gamma \tag{3.21}$$

where $\rightarrow$ should be read as "is replaced by". Note that the leading terms of the asymptotic expansions of both the right and left handsides of Eqs. (3.20) and (3.21) are equal. Assuming that $R_r(\gamma)$ and $T_r(\gamma)$ characterize the crack, the reflected and transmitted leaky Rayleigh wavefields are readily constructed. Finally, ray tracing is used to partition the surface as indicated in Figs. (3.6) through (3.8) and as denoted by the various Heaviside step functions $u(x)$ in Eqs. (3.17)-(3.19). The (-1) terms are needed to remove the incident Rayleigh waves from regions where they are no longer present. To obtain the net scattered wavefield, the result in Eq. (3.6) is added to Eq. (3.17) and the result in Eq.(3.7) is added to Eqs. (3.18)-(3.19). Several approximations were carried out to derive the expressions for ϕ^s_{cr} many of which are to be justified on physical grounds. Nevertheless, there is confidence that the essential propagation processes have been captured.

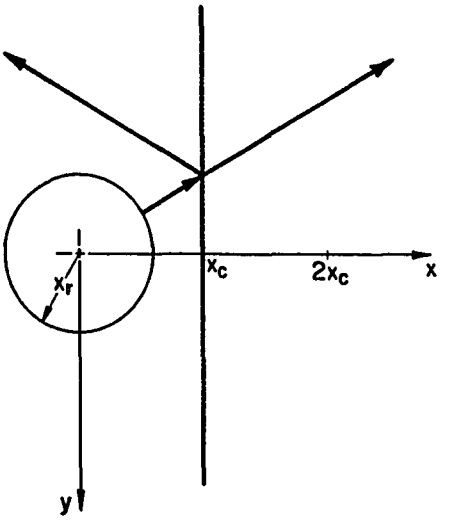

Fig. 3.7 A ray tracing of the crack scattered wavefield on the interface when the geometrical focal point lies above the interface and $x_r < x_c$. A typical set of rays is shown.

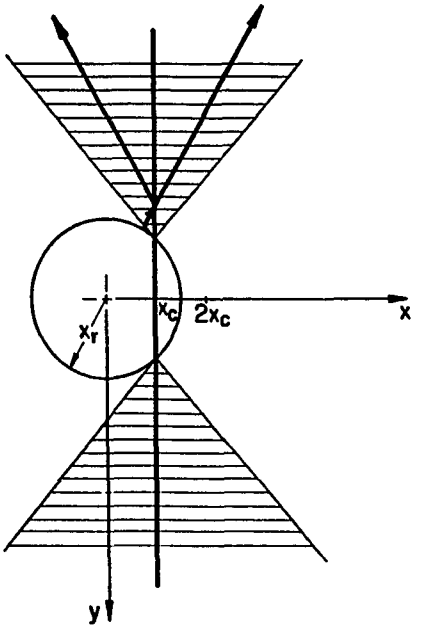

Fig. 3.8 A ray tracing of the crack scattered wavefield on the interface when the geometrical focal point lies above the interface and $x_r > x_c$. A typical set of rays is shown. The shaded regions indicate those accessible to the reflected and transmitted rays.

Figure 3.9 shows a transverse profile for the total scattered wavefield in the plane of the lens' aperture $z = -f$ where the geometrical component has undergone sufficient decay so that the presence of the several scattered Rayleigh waves is clear. The solid is fused quartz. The same values for the parameters as have been used in the previous figures are used here. The crack is located at $x_c/b = 0.02$. The scattered wavefield is no longer axisymmetric due to the placement of the crack into the surface. For ease of illustration, the scattered wavefield has been plotted along the x-axis. Instead of numerically integrating Eq. (3.17), the expression was asymptotically approximated in a non-uniform manner. This will produce two singularities in Fig. 3.9 placed at the focal points of the leaky Rayleigh wavefield namely at $x = 0, 2x_c$ on the interface. These will be shifted along the x-axis by the amount $|f - z_s| \tan \beta_r$ in the lens' aperture. The crack reflection and transmission coefficients for a leaky Rayleigh wave, $R_r(\gamma) = 0.4 e^{i0.6}$ and $T_r(\gamma) = 0$, have been assumed to be that for a deep crack with no fluid loading. They have also been chosen to have no angle dependence as a first approximation of the problem. These values have been taken from Achenbach, *et al.* (1980) and they were also used in Chap. 2. Comparison of Fig. 3.9 with Fig. 3.2 shows that the presence of the crack has considerable influence on the scattered wavefield.

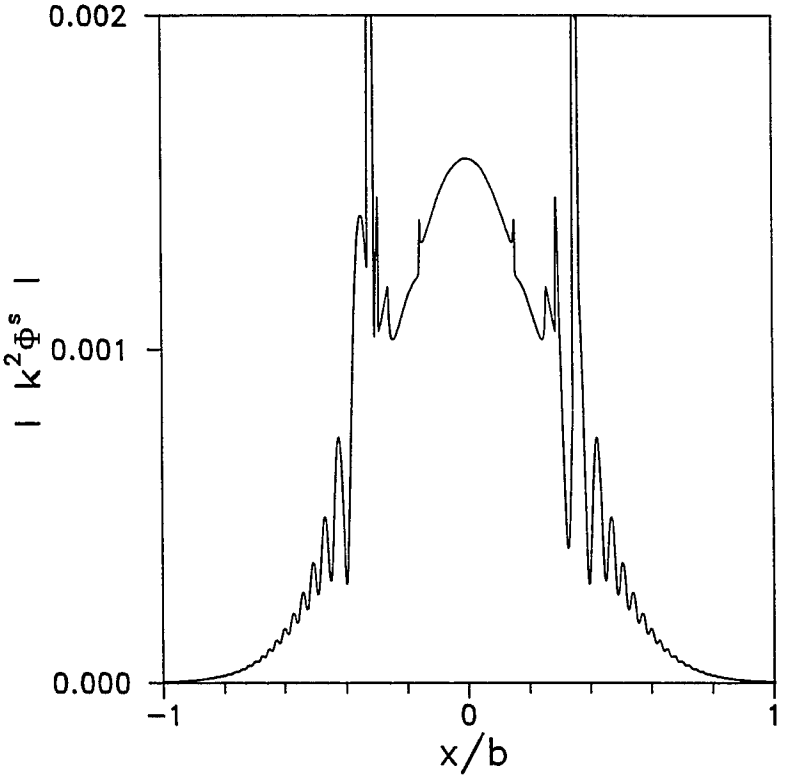

Fig. 3.9 Transverse profile of the scattered wavefield along the lens' aperture at a defocus of $z_s/\lambda_w = -10$ for fused quartz with a surface-breaking crack at $x_c/b = 0.02$. The incident profile parameters are $n = 1$ and $a/b = 0.50$.

3.5.2 The Perturbation in the Acoustic Signature

As Eqs. (3.10), (3.11) and (3.13) suggest, the net acoustic signature for a specimen containing a surface-breaking crack can be written as

$$\delta V = \delta V_o + \delta V_{cr} \tag{3.22}$$

where δV_o is the contribution from the geometrically reflected wavefield plus that from the leaky Rayleigh wavefield when no crack is present, and δV_{cr} is the contribution caused by the presence of the crack. Usually only $|\delta V|$ can be measured because it is difficult to make accurate phase measurements at high frequencies. However, work by Liang, *et al.* (1985b) and Reinholdtsen and Khuri-Yakub (1991) suggests that this problem can be overcome, and that the magnitude and the phase of δV can be measured. If we assume that δV_o is measured in a region of the surface unaffected by Rayleigh waves scattered by the crack, then a measurement of δV allows $|\delta V_{cr}| = |\delta V - \delta V_o|$ to be measured. Using the approximate wavefields, Eqs. (3.17)-(3.19), in combination with an asymptotic approximation to the incident wavefield Eq. (3.1), δV_{cr} is calculated using Eq. (1.1).

The surface S needs to be selected. Both the plane of the lens' aperture and the interface could be used. However, the interface is simpler to work with. Accordingly, δV_{cr}^{P} for the geometrical focal point below the surface is given by the following integral evaluated over the interface.

$$\delta V_{cr}^{P} = \frac{1}{\pi} C^{P} k \,|\, z_s \,|\, \alpha_r \sin\beta_r \, G(\beta_r) \exp(-ikbF \,|\, \bar{z}_s \,|\, \cos\beta_p)$$

$$\times \{ \int_{-\pi}^{\pi} \int_{0}^{\beta_a} \int_{-\frac{\pi}{2}}^{\frac{\pi}{2}} u(x_c - x) H(\beta) R_r(\gamma) \exp[ikb\, Q_R^{+}(\beta, \phi, \gamma)] \, d\gamma d\beta d\phi$$

$$+ \int_{-\pi}^{\pi} \int_{0}^{\beta_a} \int_{-\frac{\pi}{2}}^{\frac{\pi}{2}} u(x - x_c) H(\beta) [T_r(\gamma) - 1] \exp[ikb\, Q_T^{+}(\beta, \phi, \gamma)] d\gamma d\beta d\phi$$

$$+ u(x_r - x_c) \int_{-\pi}^{\pi} \int_{0}^{\beta_a} \int_{-\frac{\pi}{2}}^{\frac{\pi}{2}} u(x - x_c) u\left(|2 - \frac{x}{x_c}| - |\frac{y}{\sqrt{x_r^2 - x_c^2}}| \right)$$

$$\times H(\beta) R_r(\gamma) \exp[ikb\, Q_R^{-}(\beta, \phi, \gamma)] \, d\gamma d\beta d\phi$$

$$+ u(x_r - x_c) \int_{-\pi}^{\pi} \int_{0}^{\beta_a} \int_{-\frac{\pi}{2}}^{\frac{\pi}{2}} u(x_c - x) u\left(|\frac{x}{x_c}| - |\frac{y}{\sqrt{x_r^2 - x_c^2}}| \right)$$

$$\times H(\beta) [T_r(\gamma) - 1] \exp[ikb\, Q_T^{-}(\beta, \phi, \gamma)] d\gamma d\beta d\phi \} \qquad (3.23)$$

The functions $H(\beta)$, $Q_I^{\pm}(\beta, \phi, \gamma)$ where I indicates R, T which are the reflected and transmitted signals respectively, are given as

$$H(\beta) = G(\beta) \tan\beta \left(1 + \frac{\cos\beta_r}{\cos\beta} \right) \qquad (3.24)$$

and

$$Q_R^{\pm}(\beta, \phi, \gamma) = \pm \bar{x}_c \sin\beta_p \cos\gamma - F \,|\, \bar{z}_s \,|\, [\sec\beta \pm \sin\beta_p \tan\beta \cos(\phi + \gamma)] \qquad (3.25)$$

$$Q_T^{\pm}(\beta, \phi, \gamma) = F \,|\, \bar{z}_s \,|\, [-\sec\beta \pm \sin\beta_p \tan\beta \cos(\phi - \gamma)] \,. \qquad (3.26)$$

Also, $x = |z_s| \tan\beta\cos\phi$, $y = |z_s| \tan\beta\sin\phi$ and $x_r = |z_s| \tan\beta_r$. Similiarly, δV_{cr}^P, for the geometrical focal point above the surface, is given by the following integral evaluated along the interface for $x_r < x_c$.

$$\delta V_{cr}^P = -\frac{1}{\pi} C^P k |z_s| \alpha_r \sin\beta_r G(\beta_r) \exp(ikbF|\bar{z}_s|\cos\beta_p)\, u(x_c - x_r)$$

$$\times \{ \int_{-\pi}^{\pi} \int_{0}^{\beta_a} \int_{-\frac{\pi}{2}}^{\frac{\pi}{2}} u(x_c - x) H(\beta) R_r(\gamma) \exp[-ikb Q_R^-(\beta,\phi,\gamma)]\, d\gamma d\beta d\phi$$

$$+ \int_{-\pi}^{\pi} \int_{0}^{\beta_a} \int_{-\frac{\pi}{2}}^{\frac{\pi}{2}} u(x - x_c) H(\beta) [T_r(\gamma) - 1] \exp[-ikb Q_T^-(\beta,\phi,\gamma)] d\gamma d\beta d\phi \} \qquad (3.27)$$

And, for $x_r > x_c$, one obtains

$$\delta V_{cr}^P = -\frac{1}{\pi} C^P k |z_s| \alpha_r \sin\beta_r G(\beta_r) \exp(ikbF|\bar{z}_s|\cos\beta_p)\, u(x_r - x_c)$$

$$\times \{ \int_{-\pi}^{\pi} \int_{0}^{\beta_a} \int_{-\frac{\pi}{2}}^{\frac{\pi}{2}} u(x_c - x)\, u\left(\left| \frac{y}{\sqrt{x_r^2 - x_c^2}} \right| - \left| 2 - \frac{x}{x_c} \right| \right)$$

$$\times H(\beta) R_r(\gamma) \exp[-ikb Q_R^-(\beta,\phi,\gamma)]\, d\gamma d\beta d\phi$$

$$+ \int_{-\pi}^{\pi} \int_{0}^{\beta_a} \int_{-\frac{\pi}{2}}^{\frac{\pi}{2}} u(x - x_c)\, u\left(\left| \frac{y}{\sqrt{x_r^2 - x_c^2}} \right| - \left| \frac{x}{x_c} \right| \right)$$

$$\times H(\beta) [T_r(\gamma) - 1] \exp[-ikb Q_T^-(\beta,\phi,\gamma)] d\gamma d\beta d\phi \}. \qquad (3.28)$$

In these expressions, the distances x_c and x_r were defined earlier. Also, in contrast to similiar expressions given by Somekh, *et al.* (1985) and Li, *et al.* (1991), these are given as integrals in physical space instead of wavenumber space. By working in physical space the partitioning of the surface can be done in a relatively simple manner.

The exponential terms in the expressions for δV_{cr}^P, Eqs. (3.23), (3.27) and (3.28), have been scaled in order that we may asymptotically approximate them to obtain an estimate of the form of δV_{cr}^P. The earlier work in Chap. 2 suggests that such approximations can be accurate. Doing so gives, for the focal point below the interface,

$$\delta V_{cr}^P = -4\pi i\, C^P\, \alpha_r \sin\beta_r\, G^2(\beta_r) \exp(-i2k\,|\,z_s\,|\cos\beta_p)$$
$$\times\{\frac{R_r(0)}{\sqrt{\pi k x_c \sin\beta_r}}\left[\exp\left(i2kx_c\sin\beta_p - i\frac{\pi}{4}\right) + u(x_r - x_c)\exp\left(-i2kx_c\sin\beta_p + i\frac{\pi}{4}\right)\right]$$
$$+\sqrt{2}\,u(x_r - x_c)\exp\left(i\frac{\pi}{4}\right)(T_M - U_M)\} \tag{3.29}$$

and for $x_c = 0$, which is a special case,

$$\delta V_{cr}^P = -8\pi i\, C^P\, \alpha_r \sin\beta_r\, G^2(\beta_r)\,(R_M + T_M - 1)\exp(-i2k\,|\,z_s\,|\cos\beta_p). \tag{3.30}$$

For the focal point above the interface, one obtains

$$\delta V_{cr}^P = -4\pi i\, C^P\, \alpha_r \sin\beta_r\, G^2(\beta_r) \exp(i2k\,|\,z_s\,|\cos\beta_p)$$
$$\times\frac{R_r(0)}{\sqrt{\pi k x_c \sin\beta_r}}u(x_c - x_r)\exp\left(i2kx_c\sin\beta_p - i\frac{\pi}{4}\right). \tag{3.31}$$

In the above expressions, R_M is the mean crack reflection coefficient,

$$R_M = \frac{2}{\pi}\int_0^{\frac{\pi}{2}} u(\phi_c - \phi) R_r(\phi)\, d\phi \tag{3.32}$$

T_M is the mean crack transmission coefficient,

$$T_M = \frac{2}{\pi}\int_0^{\frac{\pi}{2}} u(\phi_c - \phi) T_r(\phi)\, d\phi \tag{3.33}$$

and U_M is the mean Heaviside function

$$U_M = \frac{2}{\pi}\int_0^{\frac{\pi}{2}} u(\phi_c - \phi)\, d\phi \quad = \quad \frac{2}{\pi}\phi_c \tag{3.34}$$

where $\phi_c = \cos^{-1}(x_c/x_r)$ for $x_c < x_r$. When $x_c > x_r$, the Heaviside function in Eq. (3.29) is zero and there is no contribution from the $T_M - U_M$ term.

These results can be compared to those for the line focus lens which was discussed in Chap. 2. First, for the focal point below the interface, Eq. (2.25),

$$\begin{aligned} \delta V_{cr}^L = {} & 4\pi i C^L \alpha_r E^2(\beta_r) \exp(-i2k\,|\,z_s\,|\cos\beta_p) \\ & \times \{R_r(0)\,[\exp(i2kx_c \sin\beta_p) + u(x_r - x_c)\exp(-i2kx_c \sin\beta_p)] \\ & + 2u(x_r - x_c)\,[T_r(0) - 1]\} \end{aligned} \tag{3.35}$$

and secondly, for the focal point above the interface, Eq. (2.26),

$$\delta V_{cr}^L = 4\pi i C^L \alpha_r E^2(\beta_r) \exp(i2k\,|\,z_s\,|\cos\beta_p)\, R_r(0)\, u(x_c - x_r) \exp(i2kx_c \sin\beta_p)\,. \tag{3.36}$$

In Figs. 3.10 through 3.13, the acoustic signature for a specimen containing a surface-breaking crack calculated using a crack with a point focus lens is compared to that determined using a line focus lens. The material is fused quartz in all cases. Although they exhibit the same interference pattern, their magnitudes differ. Figures 3.10 and 3.12 illustrate $|\delta V_{cr}|$ as x_c/b is varied. Figures 3.11 and 3.13 show the dependence of the difference in the magnitudes of the total crack perturbed output voltage with that of a defect-free surface ($|\delta V|-|\delta V_o|$) on the position of the surface-breaking crack x_c/b. In Figs. 3.10 and 3.11, the microscope is at a defocus of $z_s/\lambda_w = 5$, while in Figs. 3.12 and 3.13 the defocus is $z_s/\lambda_w = -10$.

As used and discussed in section 2.5.2, the crack reflection and transmission coefficients for a leaky Rayleigh wave are $R_r(\gamma) = 0.4e^{i0.6}$ and $T_r(\gamma) = 0$. These coefficients approximate those for a deep crack whose faces are not in mechanical contact. Further, it was assumed that they have no dependence on the angle of incidence. Despite their simplicity, the choice of these coefficients gives a good overall picture of how $|\delta V_{cr}|$ depends on each. The crack reflection coefficient primarily effects the oscillation of the signal as seen in the first term of Eq.(3.29) while the crack transmission coefficient effects the magnitude of the signal for $x_c < x_r$ as observed in the second term of Eq. (3.29). This is illustrated in Figs. 3.12 and 3.13. For $x_c > x_r$, the signal $|\delta V_{cr}|$ is dependent on only the crack reflection coefficient as noted by Eq. (3.31) and 3.10 and 3.11. Therefore, the asymptotic results given by Eqs. (3.29), (3.31), (3.35) and (3.36) reproduce the dependence of the crack perturbed acoustic signature on the crack reflection and transmission coefficients as experimentally observed by Rowe, *et al.* (1986).

The ripples for $x_c > x_r$ in both Figs. 3.11 and 3.13 are spaced approximately $\lambda_r/2$ apart indicating that a standing wave pattern has been established. This agrees with the long range behavior observed by Yamanaka and Enomoto (1982). It is also observed that the crack

perturbed acoustic signature using a point focus lens $|\,\delta V_{cr}^{P}\,|$, Eq. (3.31), is identical in form to the result using a line focus lens $|\,\delta V_{cr}^{L}\,|$, Eq. (3.36), except for a decrease in the signal strength as observed in Figs. 3.10 and 3.11 for a defocus of $|\,z_s\,|/\lambda_w = 5$ when $x_c > x_r$.

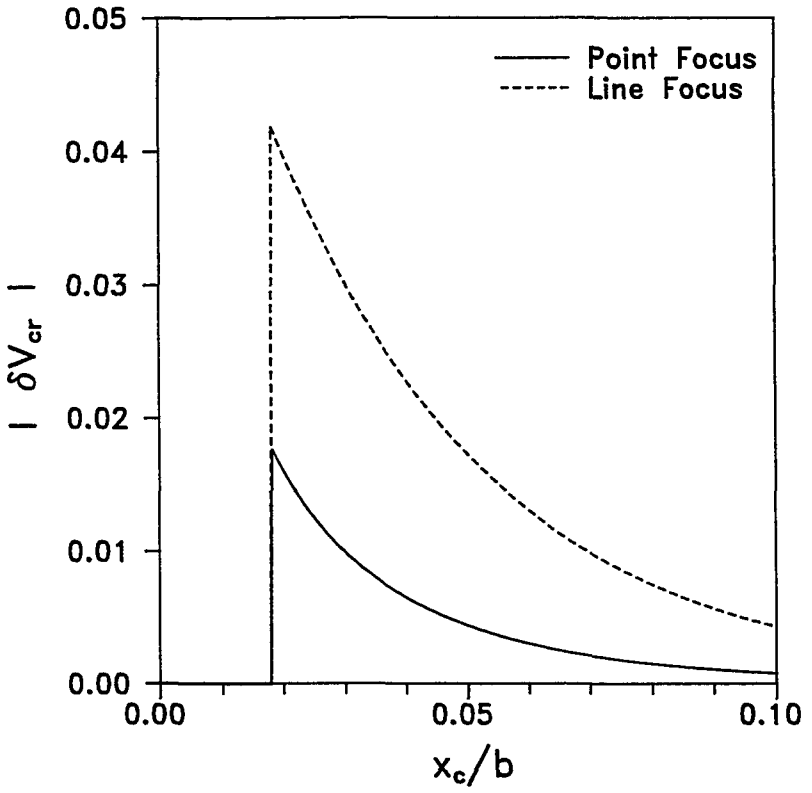

Fig. 3.10 The magnitude of that part of the acoustic signature caused by the presence of a surface-breaking crack located at x_c at a defocus of $z_s/\lambda_w = 5$ for fused quartz. The incident profile parameters are $n = 1$ and $a/b = 0.50$.

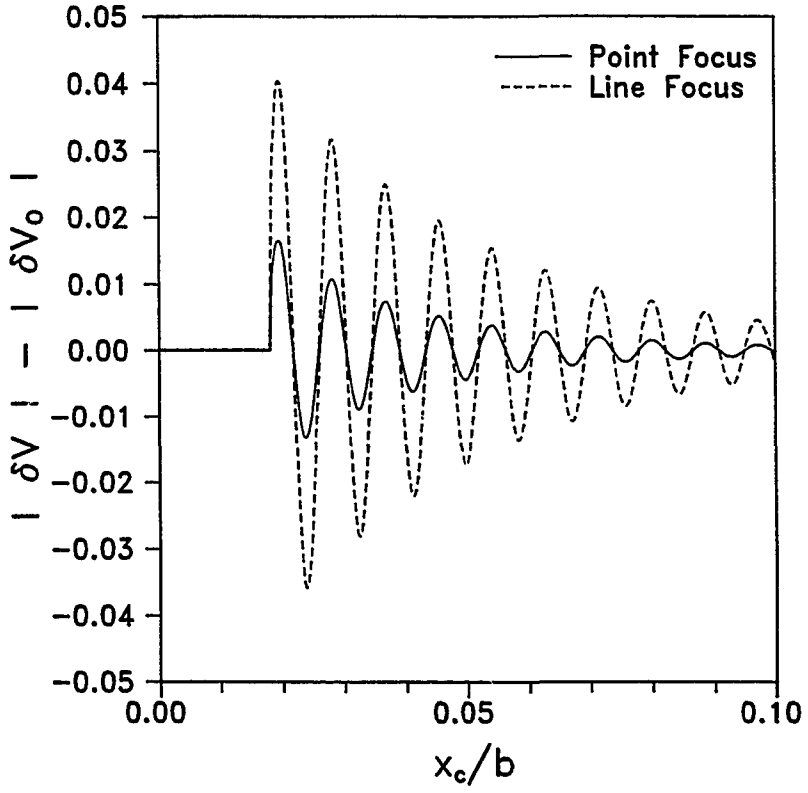

Fig. 3.11 The difference $|\delta V| - |\delta V_o|$ caused by the presence of a surface-breaking crack located at x_c at a defocus of $z_s/\lambda_w = 5$ for fused quartz. The incident profile parameters are $n = 1$ and $a/b = 0.50$.

The strong ripples for $x_c < x_r$ in Fig. 3.12 indicate why surface features stand out so vividly in acoustic images. This agrees with the short range behavior observed by Ilett, *et al.* (1984). In this figure, the crack perturbed acoustic signature using a point focus lens $|\,\delta V_{cr}^{P}\,|$, Eq. (3.29), agrees in basic form to the result using a line focus lens $|\,\delta V_{cr}^{L}\,|$, Eq. (3.35), except for a decay in signal strength as the crack is moved further off axis when using a point focus lens.

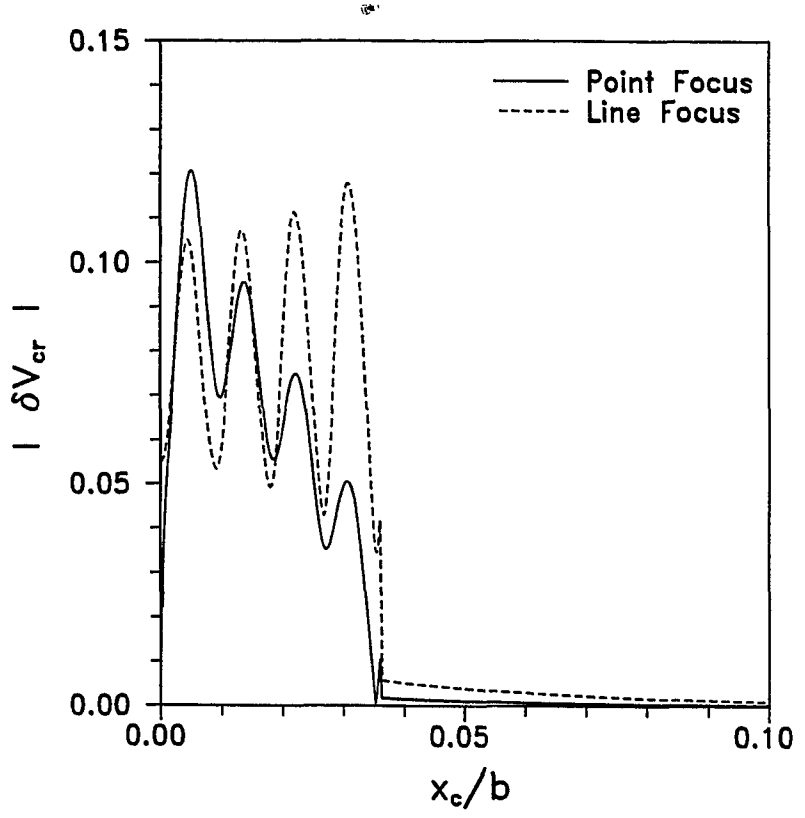

Fig. 3.12 The magnitude of that part of the acoustic signature caused by the presence of a surface-breaking crack located at x_c at a defocus of $z_s/\lambda_w = -10$ for fused quartz. The incident profile parameters are $n = 1$ and $a/b = 0.50$.

In Fig. 3.13, the point focus and line focus results for ($|\delta V|-|\delta V_o|$) are dissimiliar in magnitude when $x_c < x_r$. This could be due to a shift in the interference pattern of the acoustic signature for a defect-free surface when comparing point focus to line focus microscopes (Fig. 3.5).

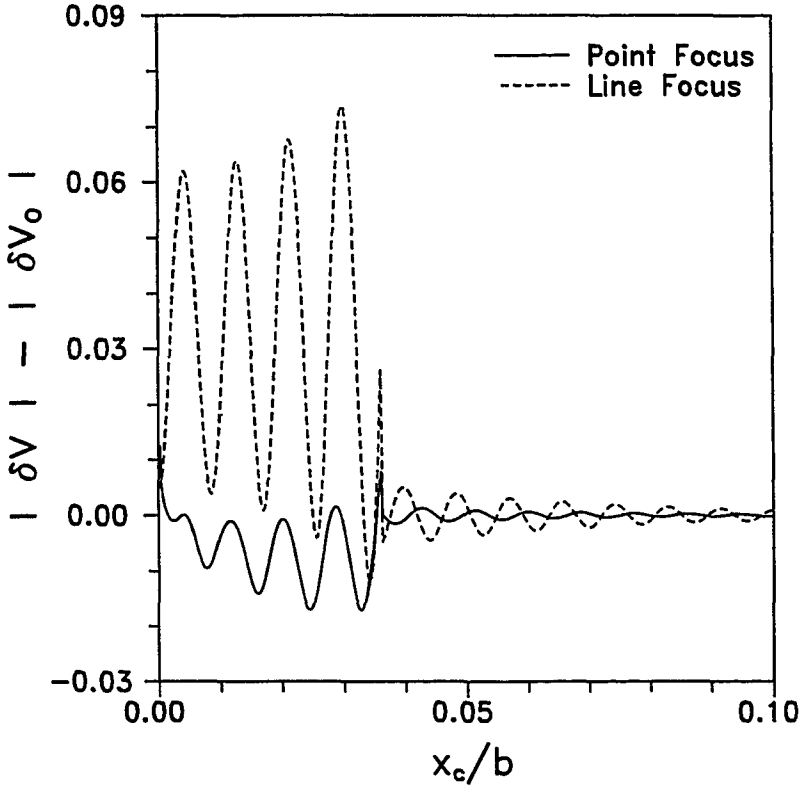

Fig. 3.13 The difference $|\delta V|-|\delta V_o|$ caused by the presence of a surface-breaking crack located at x_c at a defocus of $z_s/\lambda_w = -10$ for fused quartz. The incident profile parameters are $n = 1$ and $a/b = 0.50$.

In Fig. 3.14, the line focus result is calculated at a defocus of $z_s/\lambda_w = -9.5$. The decrease in defocus of 0.5 corresponds to the shift observed in Fig. 3.5. The curves now agree in basic form but differ in magnitude of the oscillation. This diminished signal strength also occured for the positive defocus case shown in Fig. 3.11. It should be noted that shifting to a defocus of $z_s/\lambda_w = -9.5$ does not greatly alter $|\delta V_{cr}^{L}|$ shown in Fig. 3.12. In the region $x_c < x_r$, the oscillations for both the point focus and line focus lenses are in phase.

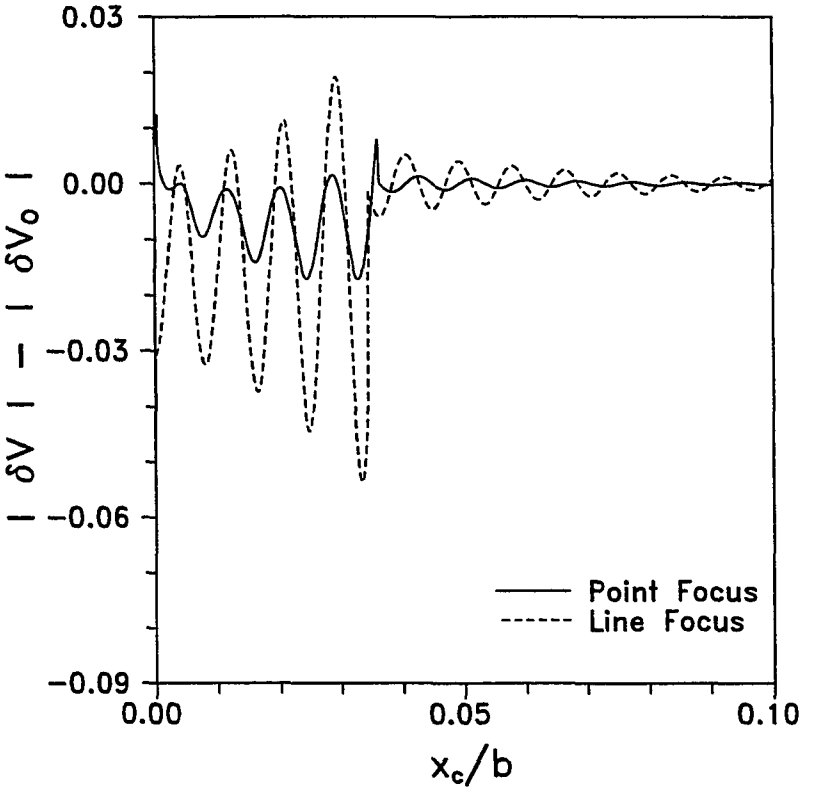

Fig. 3.14 The difference $|\delta V| - |\delta V_o|$ caused by the presence of a surface-breaking crack located at x_c in fused quartz at a defocus of $z_s/\lambda_w = -10$ for the point focus lens compared to $z_s/\lambda_w = -9.5$ for the line focus lens.

This shift between comparisons of the theoretical crack perturbed acoustic signature from a line focus microscope to that of an experimentally obtained one from a point focus microscope has been previously attributed to thermal drift, the measurement of z, and the frequency and beam profile used (Briggs, 1990). From this work, it could also be caused by differences in geometry of the two microscopes. Namely, the order of the geometrical contribution of the line focus lens in comparison to that of a point focus lens.

CHAPTER 4

Conclusions

A model has been constructed of the line focus and the point focus acoustic microscopes using asymptotic methods that reproduce the basic features of the acoustic signature and many of the mathematical expressions derived by others. This method of approach allows one to determine the acoustic signature of a surface-breaking crack in a relatively simple manner and it can be extended to take account of other surface structures. Moreover, explicit expressions were obtained for the various wavefields and acoustic signatures.

The differences in the acoustic signatures determined using a line focus or point focus lens were shown not to be large qualitatively for a defect-free surface and for one containing a surface-breaking crack. However, there were quantitative differences in their relative magnitudes and interference patterns.

An estimate of the crack reflection and transmission coefficients can be determined using either a line focus or point focus lens when an experimental crack perturbed acoustic signature δV_{cr} has been measured. While these calculations depend upon an ability to measure the magnitude and the phase of both δV and δV_o, the prospect of such a measurement is of great interest. Note that δV_{cr} is the vector difference of δV, the total acoustic signature with a surface-breaking crack, and δV_o which is the acoustic signature for the surface far from the effects of the surface-breaking crack.

For example, from Eqs. (2.26) and (2.27), for $x_c > x_r$ using a line focus microscope, an estimate of the reflection coefficient $R_r(0)$ can be calculated, giving

$$R_r(0) = \delta V_{cr}^{L} \left\{ \frac{\exp[-i2k(x_c \sin\beta_p \pm |z_s| \cos\beta_p)]}{-4\pi C^L \alpha_r E^2(\beta_r)} \right\} \tag{4.1}$$

whereas the reflection coefficient for a surface-breaking crack using a point focus microscope, Eqs. (3.29) and (3.31), can be written as

$$R_r(0) = \delta V_{cr}^{P} \sqrt{\frac{\pi k x_c}{\sin\beta_r}} \exp\left(-i\frac{\pi}{4}\right) \left\{ \frac{\exp[-i2k(x_c \sin\beta_p \pm |z_s| \cos\beta_p)]}{-4\pi C^P \alpha_r G^2(\beta_r)} \right\} \tag{4.2}$$

where the plus sign indicates that the focal point lies above the interface and the minus sign indicates that it lies below. Once $R_r(0)$ has been measured, a second output voltage is obtained using $x_c < x_r$ to determine either $T_r(0)$ from Eq. (2.26) or T_M from Eq. (3.29) depending whether or not a line focus or point focus lens is being used with the scanning acoustic microscope to make the measurements.

Because $R_r(0)$ is a function primarily of d/λ_r and the material properties, the crack depth d could be extracted from a measurement of $R_r(0)$. Alternatively, a basis for characterizing surface-breaking cracks could be established using a measurement of R_r.

APPENDIX A

The Complex β-Plane

The reflection coefficient $R(\beta)$, when attenuation is not accounted for, is given by

$$R(\beta)=\frac{A_{-}(\beta)}{A_{+}(\beta)} \tag{A1}$$

where

$$A_{\pm}(\beta)=\left(\frac{c_T}{c}\right)^2\cos\beta\left\{4\sin^2\beta\, a_L(\beta)\, a_T(\beta)+\left[\left(\frac{c}{c_T}\right)^2-2\sin^2\beta\right]^2\right\}\pm\rho\, a_L(\beta)\left(\frac{c}{c_T}\right)^2 \tag{A2}$$

and

$$a_I(\beta)=\sqrt{\left(\frac{c}{c_I}\right)^2-\sin^2\beta}\,, \qquad Im\{a_I(\beta)\}\geq 0\;\forall\,\beta\,. \tag{A3}$$

The subscript I is replaced with L or T for a_L or a_T respectively. The terms c_L and c_T are the longitudinal and transverse wavespeeds for the solid respectively; c is the wavespeed for the fluid. The parameter $\rho=\rho_f/\rho_s$ where ρ_f is the fluid density and ρ_s is that for the solid. The definition of the radicals is determined by demanding that the reflected waves propagate or evanesce away from the interface.

Figure A.1 shows how the complex β-plane is cut to achieve this requirement. Also shown is the integration contour for Eqs. (2.8) and (3.5).

Note that in quadrants 2 and 4, $Im(\cos\beta)\geq 0$ and $Im(a_I)\geq 0$, while in quadrants 1 and 3, $Im(\cos\beta)\leq 0$ and $Im(a_I)\geq 0$. Therefore to approximate asymptotically the integral given in Eqs.

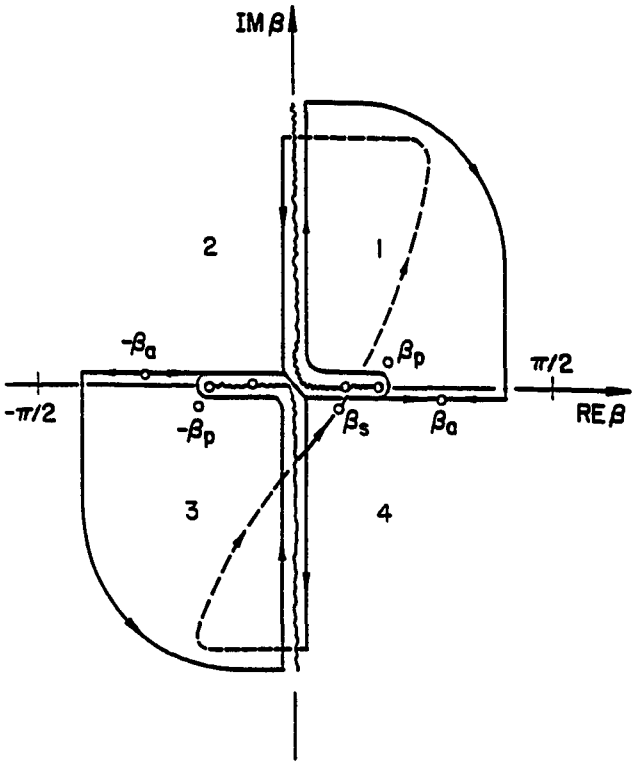

Fig. A.1 A sketch of the complex β-plane showing the critical points the contours of integration.

(2.8) and (3.5) for a disturbance outgoing from the reflected focal plane, the steepest descent path must traverse portions of quadrants 2 and 4. However, for a disturbance incoming to the reflected focal plane the steepest descent path sketched in Fig. A.1 is appropriate. The solid line indicates those portions on the Riemann sheet defined by Eq. (A3), while the dashed line indicates the path on the lower sheet. Note that we place the saddle point β_s on the Riemann sheet defined by Eq. (A3). Further, note that the leaky Rayleigh wave poles are surrounded when the wave is incoming to the reflected focal plane. This is the general scheme is used for all the asymptotic evaluations.

REFERENCES

Achenbach, J.D., Ahn, V.S. and Harris, J.G. (1991) Wave analysis of the acoustic signature of a line focus microscope. *IEEE Trans. Ultrason. Ferroelect. Freq. Cont.*, **34**: 380-387.

Achenbach, J.D., Gautesen, A.K. and Mendelsohn, D.A. (1980) Ray analysis of surface-wave interaction with an edge crack. *IEEE Trans. Sonics Ultrason.* **SU-27**: 124-129.

Angel, Y.C. and Achenbach, J.D. (1984) Reflection and transmission of obliquely incident Rayleigh waves by a surface-breaking crack. *J. Acoust. Soc. Am.* **75**: 313-319.

Ahn, V.S., Harris, J.G. and Achenbach, J.D. (1991) Numerical analysis of the acoustic signature of a surface-breaking crack. *IEEE Trans. Ultrason. Ferroelect. Freq. Cont.*, to appear.

Auld, B.A. (1979) General electromechanical reciprocity relations applied to the calculation of elastic wave scattering coefficients. *Wave Motion* **1**: 3-10.

Bertoni, H.L. (1984) Ray-optical evaluation of V(z) in the reflection acoustic microscope. *IEEE Trans. Sonics Ultrason.* **SU-31**: 105-116.

Brekhovskikh, L.M. (1980) *Waves in Layered Media*, 2nd Ed., New York: Academic.

Briggs, G.A.D. (1985) *An Introduction to Scanning Acoustic Microscopy.* New York: Oxford.

Briggs, G.A.D., Jenkins, P.J. and Hoppe, M. (1990) How fine a surface crack can you see in a scanning acoustic microscope? *Journal of Microscopy* **159**: 15-32.

Chan, K.H. and Bertoni, H.L. (1991) Ray representation of longitudinal lateral waves in acoustic microscopy. *IEEE Trans. Ultrason. Ferroelect. Freq. Cont.* **38**: 27-34.

Dong, R. and Adler, L. (1984) Measurements of reflection and transmission coefficients of Rayleigh waves from cracks. *J. Acoust. Soc. Am.* **76**: 1761-1763.

Felson, L.B. and Marcuvitz, N. (1973) *Radiation and Scattering of Waves*, Englewood Cliffs, N.J.: Prentice-Hall.

Harris, J.G. and Pott, J. (1985) Further studies of the scattering of a Gaussian beam from a fluid-solid interface. *J. Acoust. Soc. Am.* **78**: 1072-1080.

Ilett, C., Somekh, M.G. and Briggs, G.A.D. (1984) Acoustic microscopy of elastic discontinuities. *Proc. Roy. Soc. Lond.* **A 393**: 171-183.

Knopoff, L. (1969) Elastic wave propagation in a wedge. In *Wave Propagation in Solids*, ed. J. Miklowitz, pp. 3-43. New York: A.S.M.E.

Kushibiki, J.I. and Chubachi, N. (1985) Material characterization by line-focus-beam acoustic microscope. *IEEE Trans. Sonics Ultrason.* **SU-32**: 189-212.

Lawrence, C.W., Scruby, C.B., Briggs, G.A.D. and Dunhill, A. (1990) Crack detection in silicon nitride by acoustic microscopy. *NDT International* **23**: 3-10.

Lemons, R.A. and Quate, C.F. (1979) Acoustic microscopy. In *Physical acoustics*, vol. 14, eds. W.P. Mason and R.N. Thurston, pp. 1-92. New York: Academic.

Li, H.U. and Negishi, K. (1989) Visualization of ultrasonic waves propagating in scanning acoustic microscope. In *Acoustic Imaging*, vol. 17, p. 79-86. New York: Plenum.

Li, Z.L., Achenbach, J.D. and Kim, J.O. (1991) Effect of surface discontiuities on V(z) and $V(z,x_o)$ for the line-focus acoustic microscope. *Wave Motion*, to appear.

Liang, K.K., Kino, G.S. and Khuri-Yakub, B.T. (1985a) Material characterization by the inversion of V(z). *IEEE Trans. Sonics Ultrason.* **SU-32**: 213-224.

Liang, K.K., Bennett, S.D., Khuri-Yakub, B.T. and Kino, G.S. (1985b) Precise phase measurements with the acoustic microscope. *IEEE Trans. Sonics Ultrason.* **SU-32**: 266-273.

Mott, G. (1970) Reflection and refraction coefficients at a fluid-solid interface. *J. Acoust. Soc. Am.* **50**: 819-829.

Pott, J. and Harris, J.G. (1984) Scattering of a Gaussian beam from a fluid-solid interface. *J. Acoust. Soc. Am.* **76**: 1829-1835.

Rebinsky, D.A. and Harris, J.G. (1991) An asymptotic calculation of the acoustic signature of a cracked surface for the line focus scanning acoustic microscope. Submitted for review.

Reinholdtsen, P.A. and Khuri-Yakub, B.T. (1991) Image processing for a scanning acoustic microscope that measures amplitude and phase. *IEEE Trans. Ultrason. Ferroelect. Freq. Cont.* **38**: 141-147.

Rowe, J.M., Kushibiki, J.I., Somekh, M.G. and Briggs, G.A.D. (1986) Acoustic microscopy of surface cracks. *Phil. Trans. R. Soc. Lond.* A **320**: 201-214.

Somekh, M.G., Bertoni, H.L., Briggs, G.A.D. and Burton, N.J. (1985) A two-dimensional imaging theory of surface discontinuities with the scanning acoustic microscope. *Proc. R. Soc. Lond.* A **401**: 29-51.

Stamnes, J.J. (1986) *Waves in Focal Regions*. Bristol: Adam Hilger.

Yamanaka, K. and Enomoto, Y. (1982) Observations of surface cracks with scanning acoustic microscope. *J. Appl. Phys.* **53**: 846-850.

VITA

Douglas Alexander Rebinsky was born on May 26, 1962 in Edmonton, Alberta, Canada. In 1980, he began his collegiate studies. He earned a B.Sc. in Mechanical Engineering in 1984 and a M.Sc. in Mechanical Engineering in 1986 at the University of Alberta. For his master's, he obtained a general working knowledge of the mechanical behavior of materials with a special interest in metal fatigue as related to surface improvement. He moved to the University of Illinois in the fall of 1986 to join the Department of Theoretical and Applied Mechanics. After some initial work concerning the fracture of modern materials, he decided to study problems of wave propagation as applied to scanning acoustic microscopy under the direction of Professor John G. Harris. This work was completed in the summer of 1991 with a Ph.D. to be awarded in the fall of 1991. At this time, he has broad analytical skills in the areas of mechanical behavior of materials, fracture mechanics of modern materials and wave propagation.

Publications:

Rebinsky, D.A. and Harris, J.G. (1991) An asymptotic estimate of the acoustic signature for a surface-breaking crack produced by a point focus microscope. Submitted for review to *Proc. Roy. Soc. Lond.*

Rebinsky, D.A. and Harris, J.G. (1991) An asymptotic calculation of the acoustic signature of a cracked surface for the line focus scanning acoustic microscope. Submitted for review to *Proc. Roy. Soc. Lond.*

Rebinsky, D.A. and Harris, J.G. (1991) An asymptotic description fo the acoustic material signature, In *Proc. CANCAM'91*, eds. N. Popplewell and A.H. Shaw, Winnipeg, Canada: Univ. of Manitoba, 1: 262-263.

Rebinsky, D.A. and Harris, J.G. (1991) QNDE of thin metal films using the scanning laser acoustic microscope. In *Review of Progress in Quantitative Nondestructive Evaluation*, eds. D.O. Thompson and D. Chimenti, New York: Plenum, **10A**: 1043-1049.